SYNTHESIS AND CHARACTERIZATION OF COLLOIDAL QUANTUM WELLS: FROM SIMPLE SIZE-TUNED CORE TO COMPLEX MULTI-CROWN STRUCTURES

A THESIS SUBMITTED TO

THE GRADUATE SCHOOL OF ENGINEERING AND SCIENCE

OF BILKENT UNIVERSITY

IN PARTIAL FULFILLMENT OF THE REQUIREMENTS FOR

THE DEGREE OF

MASTER OF SCIENCE

IN

MATERIALS SCIENCE AND NANOTECHNOLOGY

By
Didem Dede
August 2018

SYNTHESIS AND CHARACTERIZATION OF COLLOIDAL QUANTUM WELLS: FROM SIMPLE SIZE-TUNED CORE TO COMPLEX MULTI-CROWN STRUCTURES

By Didem Dede

August 2018

We certify that we have read this thesis and that in our opinion it is fully adequate, in scope and in quality, as a thesis for the degree of Master of Science.

———————————————————
Hilmi Volkan Demir(Advisor)

———————————————————
Bilge Baytekin

———————————————————
Muhsine Bilge İmer

Approved for the Graduate School of Engineering and Science:

———————————————————
Ezhan Karaşan
Director of the Graduate School

ABSTRACT

SYNTHESIS AND CHARACTERIZATION OF COLLOIDAL QUANTUM WELLS: FROM SIMPLE SIZE-TUNED CORE TO COMPLEX MULTI-CROWN STRUCTURES

Didem Dede

M.S. in Materials Science and Nanotechnology

Advisor: Hilmi Volkan Demir

August 2018

As a new class of semiconductor nanocrystals, colloidal quantum wells (CQWs), also commonly known as nanoplatelets (NPLs), exhibit remarkable electronic and optical properties that will potentially find a wide range of use from nanophotonics to optoelectronics. NPLs feature step-like absorption profiles and discrete emission spectra with giant oscillator strength resulting in high recombination rates. All these features make these atomically-flat structures highly attractive for light-harvesting and -generating applications. In this thesis, to understand the size-tuned properties of their two-dimensional architecture, we conducted a systematic study on the core-only NPLs by using a set of 4 monolayer (ML) CdSe cores as our working model and carefully altered their aspect ratio while keeping their lateral area constant. In such a core-only NPL structure, electron and hole are both confined in the core resulting in type-I electronic band alignment. By decreasing the width of these NPLs to a value comparable to or less than their exciton Bohr radius, we observe additional confinement effects emerge. Subsequently, by growing $CdSe_{1-x}Te_x$ alloyed crown around these starting 4 ML CdSe cores, we find type-II electronic band alignment is obtained. Thanks to their spatially indirect excitons, these core crown NPLs show extraordinarily long radiative lifetimes. Moreover, with the increased absorption cross-section owing to their added crown, high-performance optical gain is achieved via their core/crown heterostructure. However, in this form, their usage is limited since they are unstable in solution forming gels and they exhibit strong tendency to form stacks in films. To address this problem, here we proposed and developed a multi-crown architecture by additionally growing a CdS crown around the periphery of the type-II heterostructure, enabling excellent optical gain media with enhanced stability. The structural and optical characterizations of the synthesized multi-crown NPLs

indicate that this complex architecture holds great promise for making devices in colloidal nanophotonics and optoelectronics.

ÖZET

KOLOİDAL KUANTUM KUYULARININ SENTEZİ VE KARAKTERİZASYONU: BASİT BOYUTLARI AYARLANABİLİR ÇEKİRDEKLİDEN KARMAŞIK ÇOKLU TAÇLI YAPILARA

Didem Dede
Malzeme Bilimi ve Nanoteknoloji, Yüksek Lisans
Tez Danışmanı: Hilmi Volkan Demir
Ağustos 2018

Yarıiletken nanokristallerin yeni bir sınıfı olarak ortaya çıkan koloidal kuantum kuyuları ya da diğer adlarıyla nanolevhalar optoelektronikten nanofotoniğe kadar geniş kullanım alanları bulabilen dikkate değer elektronik ve optik özellikler sergiler. Kademeli soğurma profiline ve dar ışıma tayfına sahip olan nanolevhaların dev osilatör güçleri vardır ve bu sayede eksiton birleşim hızı yüksektir. Tüm bu özellikler ile, atomik olarak düz olan bu yapılar ışık hasatı ve üretimi uygulamaları için caziptir. Bu tezde, iki boyutlu mimariye sahip nanolevhaların boyuta bağlı özelliklerini anlamak için, 4 tek katmanlı CdSe nanolevhaları yatay alanlarını çalışma modelimiz olarak kullanarak sabit tutarken en boy oranlarını değiştirdiğimiz sistematik bir çalışma gerçekleştirdik. Bahsedilen çekirdek yapılarında, elektron ve deşiğin her ikisi de çekirdekte sınırlandırılır. Bu şekildeki yapılar tip-I elektronik bant yapısına sahiptir. Nanolevhaların genişliğinin, eksiton Bohr yarıçapa ya da daha düşük bir değere düşürülmesiyle, yapıda ek sınırlanırma etkileri gözlemledik. Ayrıca, $CdSe_{1-x}Te_x$ alaşımlı taç yapısının 4 tek katmanlı CdSe çekirdeklerin çevresinde büyütülmesiyle tip-II elektronik bant yapısı elde edilebilir. Bu sayede elektron ve deşik dalga fonksiyonları sırasıyla çekirdek ve alaşımlı taç bölgelerinde sınırlandırılır. Uzaysal indirekt eksitona sahip olmaları nedeniyle, bu çekirdek/taç yapısındaki nanolevhalar, olağanüstü uzun birleşme ömürlerine sahiptir. Ayrıca, taç yapısının büyütülmesiyle artan soğurma kesiti, yüksek performanslı optik kazanç elde edilmesine yardımcı olur. Ancak, bu malzemelerin jel oluşturacak şekilde çözelti içinde kararsız olmaları ve film halinde yan yana istiflenme eğilimleri kullanımlarını sınırlandırır. Bu problemi çözmek için, burada tip-II elektronik hetero-yapının etrafına CdS büyüterek çoklu-taç yapısında kararlı bir

mimari önerdik ve geliştirdik; bu yapı ile kararlılığı arttırılmış üstün optik kazanç sonuçları elde ettik. Yapısal ve optik karekterizasyonları yapılan bu karmaşık yapılı malzemeler, koloidal nanofotonik ve optoelektronik cihazlar için çok ümit vadetmektedir.

Anahtar sözcükler: Koloidal sentez, yarıiletken kuantum kuyuları, koloidal kuantum kuyuları, nanolevhalar, optik kazanç.

Acknowledgement

Two and a half years ago, I attended a job interview at UNAM that has led me to undertaking my MSc studies in Demir Research Group and becoming a part of UNAM family. The time I have spent here was invaluable and I would like to thank the people I have met during my graduate studies at Bilkent.

First of all, I would like to thank Prof. Hilmi Volkan Demir, my supervisor, for his great guidance towards my MSc degree. He has been a great model to me and his boundless motivation to do research pushed me forward on the path of growing into a future scientist.

I would like to thank Asst. Prof. Bilge Imer for her mentorship during my undergraduate and graduate studies. She always supported me during this whole journey. I would like to thank Asst. Prof. Bilge Baytekin for serving in my MSc thesis jury.

I would like to thank all the past and present group members. My very special thanks go to Dr. Yusuf Kelestemur, who has been my 'master' in colloidal synthesis, guiding and helping me with my research work. I would like to thank Dr. Burak Guzelturk, who motivated me to succeed in research. I would like to thank Dr. Kivanc Gungor for his answers to all my reasonable and unreasonable questions. I would like to thank Dr. Talha Erdem, Dr. Zeliha Erdem, and Dr. Aydan Yeltik for their friendship and support. I would like to thank my elder brothers Dr. Murat Olutas, Emre Unal, Ozgun Akyuz, Dr. Savas Delikanli and Dr. Manoj Sharma. I have learned many things from all of them. I would like to thank Nima Taghipour, who has become the most supportive person in my last two years. He was always being there for me when I needed help. I would like to thank Mustafa Sak, Ibrahim Tanriover, and Selim Bozdogan for their friendship and the time we have had together. I would also like to thank Onur Erdem, Ulviyya Quliyeva, Farzan Shabani, Hamza Humayun, Dr. Neghar Gheshlaghi, Dr. Yemliha Altintas, Dr. Volodymyr Sheremet, Birsen Bilgili, Dr. Evren Mutlugun,

Ekin Bircan Boşdurmaz, and Can Firat Usanmaz from our group.

During the time I have spent at UNAM, I had great friendships. I would also like to thank Ozge Begli for being such a nice flatmate. I would like to thank Musa Efe Isilak, Ugur Tegin, Engin Can Surmeli, Koray Yavuz, Onur Cakiroglu, Abtin Saateh and Abdullatif Onen for their friendship.

I would like to thank all of the faculty members, the technical and administrative staff at UNAM, who make our lives easier. I would like to especially thank Mustafa Guler, Aysegul Torun, Duygu Kazanci, Olcay Undal and Mustafa Dogan.

Finally, from the bottom of my heart, I would like to thank very much my mother Mine and my uncle Erol for their endless love, support, and encouragement throughout my life.

Contents

List of Figures

List of Tables

Chapter 1

Introduction

Developments in nanoscience and nanotechnology have led to discoveries in many fields including materials science, electronics, physics and chemistry. Understanding the quantum mechanical effects on different material types opened a new era especially in the semiconductor technology. In 1947, the first practically implemented point contact transistor was introduced by John Bardeen, Walter Brattain, and William Shockley at Bell Labs, who pioneered transistor based electronics to win Nobel Prize in Physics [3]. In 1959, Richard Feynman gave the first lecture on nanotechnology inspiring researchers on engineering at the nanoscale. The progress on these developments together with improvements on microscopy techniques have enabled expeditious advancements in nanoscience with semiconductors.

Furthermore, keeping the abreast of these developments, semiconductor growth methods have also been devised. Particularly, molecular beam epitaxy and metal organic chemical vapor deposition techniques allowed scientists to grow high crystallinity and very precise quantum structures. However, these techniques require perfect lattice matching with the substrate and they are expensive methods [4].

As a complementary approach to thin-film epitaxy methods, wet chemistry

techniques have gained importance during 1980s. In 1981, Alexei Ekimov discovered nanocrystal quantum dots in a glassy matrix [5]. He observed size-dependent optical properties of semiconducting II-VI nanocrystals. Later, Louis Brus also from Bell Labs, introduced a model for different size of CdS crystallites, [6].

These materials have then received a great attention among scientists in the late 80's owing to their unique physical properties depending on their size, shape and compositions [7],[8]. Introducing optimized wet synthesis methods led to monodisperse colloidal NCs. The first examples of monodisperse NCs include zero-dimensional (0D) cadmium-based chalcogenide quantum dots (QDs) (CdS, CdSe, CdTe), which were synthesized by Murray et al. in 1993 [9],[10]. In due time, other quantum confined structures have appeared, including one-dimensional (1D) quantum wires, and nanorods (NRs) [11], [12] and most recently, two-dimensional (2D) nanoplatelets (NPLs) [13], [14], and nanosheets [15]. All these nanomaterials exhibit different excitonic structures which result in various electronic and optical properties based on their shapes.

Besides, the excitonic properties of colloidal NCs could be tuned by altering the composition including alloying and doping. Alloying is a common technique in materials science that helps to obtain superior properties out of mixing the two similar materials. For example, by changing the sulfur amount in the $CdSe_{1-x}S_x$ NPLs, one would expect to tune the characteristics of the NPLs from pure CdSe to CdS [16]. In the doping process, impurities are introduced into the lattice to change the properties of materials [17]. For instance, CdSe NPLs are doped with Cu atoms to change the emission properties. Compared to alloying, in doping, dopant atoms are present at limited amounts and their atomic size is relatively smaller. In addition to shape and composition dependency of these materials, size has a great impact on the properties of semiconductor NCs. By changing the size of the II-VI QDs, emission can be tuned from ultraviolet (UV) to near-infrared (NIR) region.

Today, wet chemistry techniques enable us to synthesize different combinations of II-VI and III-V [18], [19], [20] of self-standing colloidal nanocrystals. Thanks to their novel photophysical features, they are used in light-emitting and

light-harvesting applications. Especially, nanocrystal-based light-emitting diodes (LEDs) have witnessed great improvement in their performance owing to their high color quality and narrow emission bandwidths [21], [22] [23], [24]. Likewise, these interesting properties of NCs make them promising candidate for lasers. There is a huge research effort continuing to make these materials as commercial lasers [25] ,[26]. Apart from light-emitting applications, nanocrystals can be used as luminophores in light-harvesting applications including solar cells [27] and luminescent solar concentrators (LSCs) [28].

In this day and age, semiconductors have been the backbone of many technological developments. The development of wet synthesis method has made the production of quantum-confined semiconductor structures more facile and cost efficient compared to thin-film epitaxy. In the last 30 years, the field of semiconductor NCs showed incredible progress and we believe that they hold great potential for many more scientific and technological advancements.

The organization of the remaning thesis is as follows. In Chapter 2, scientific background on quantum confinement and semiconductor nanocrystals is presented. Moreover, general synthesis procedure of NCs and properties of colloidal quantum wells are summarized. Chapter 3 explains the optical and structural characterization tools used extensively in this thesis for the characterization of semiconductor NPLs. In Chapter 4, we present the optical properties of our size-tuned NPLs. The synthesis method for the NPL core structure is explained in detail and their linear and nonlinear optical properties are discussed. In Chapter 5, we present our work on stabilization of Type-II NPLs. We explain our synthesis method for $CdSe/CdSe_{1-x}Te_x/CdS$ core/crown/crown NPLs and characterized their properties. Moreover, we discuss their optical gain performances in detail. In Chapter 6, we provide a conclusion.

Chapter 2

Scientific Background

2.1 Quantum Confinement

Semiconductor nanocrystals are free-standing materials that consist of clusters of hundreds to thousands of atoms. Since the size of NCs is in the range of nanometer scale, electrons and holes feel the boundary of NC structure itself resulting in the bound state of an electron and hole pairs which is called 'exciton' [29]. Exciton moves inside the crystal with a radius called exciton Bohr radius, which is a materials intrinsic property. For example, CdSe has an exciton bohr radius of 5.6 nm [30]. Therefore, if the size of the piece of a material is comparable with its exciton Bohr radius, quantum confinement effects start being observed [8]. There is a type of 1D-confined structures including nanoplatelets where only the thickness of the structure in one dimension is comparable with its exciton Bohr radius. There are also the 2D-confined structures including nanorods where exciton moves freely only in one direction and the 3D-confined structures such as QDs. All these different shapes of the semiconductors show different confinement regimes.

Among different confinement dimensionalities, quasi-zero dimensional semiconductor quantum dots are the first that have been discovered and have been

4
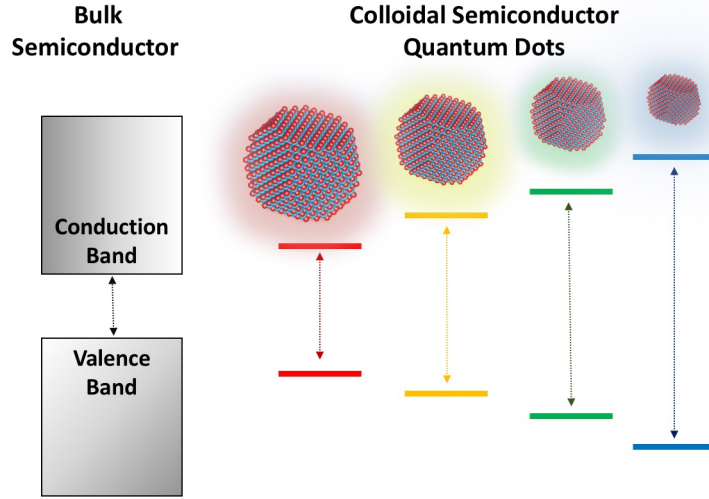
Figure 2.1: Energy band gap diagram of bulk semiconductor and its nanocrystals. The effective band gap energy increases as a result of the shrinking size of the NCs.

extensively being studied since then [9]. An exciton in quantum dots is confined in all three dimensions and their band gap has a strong dependency on their size. The decrease in the NC size results in further seperated discrete energy levels and thus increase in the effective band gap energy (Figure 1). The band gap energy of a quantum dot having radius r is given as follows

$$E_{gap}(QD) = E_{gap}(bulk) + E_{confinement} + E_{exciton} \tag{2.1}$$

$$E_{confinement} = \frac{h^2}{8\pi r^2}\left(\frac{1}{m_e} + \frac{1}{m_h}\right) \tag{2.2}$$

$$E_{exciton} = -1.8\frac{e^2}{4\pi\epsilon_0\epsilon r} \tag{2.3}$$

Here m_e and m_h are the effective masses of electron and hole, respectively. ϵ_0 is the dielectric constant in vacuum and ϵ is the relative dielectric constant of the

material (i.e. $\epsilon_0\epsilon$ is the dielectric constant of the material). Strong dependency on the size can be seen from the equations. The confinement energy ($E_{confinement}$) is proportional to $1/r^2$ whereas the exciton energy ($E_{exciton}$) is proportional to $1/r$ and $E_{exciton}$ has a reducing effect on the effective band gap energy since it is a negative value. In the strong confinement regime where both the electron and hole are tightly confined in the structure, then the confinement energy is more effective to determine the effective band gap energy of the material than the exciton energy.

2.2   Colloidal Synthesis

Colloidal synthesis of monodisperse semiconductor NCs requires three components in principal: solvent, precursors and ligands. Generally, the synthesis is performed at high temperatures so that a high boiling point solvent is necessary. Solvent could be either coordinating like trioctylphosphineoxide (TOPO) or noncoordinating like 1-Octdecene (ODE). The coordinating solvents are capable for the coordination of metal ions in the system whereas the noncoordinating solvents only provide an environment for the synthesis to take place. This is a pure homogeneous nucleation process for NCs to be formed from bare precursors. According to La Mer and Dinegar, this type of synthesis initially requires supersaturated solution, which is followed by a rapid growth procedure [31]. At the following stages of the growth, diffusion-limited Ostwald ripening occurs. As it can be seen in the Figure 2.2, when the precursors are injected rapidly, they decompose to their monomers. A sudden increase in the monomer concentration results in supersaturated solution so that the rapid nucleation takes place. When the nucleation is completed, the growth starts to proceed. The important point is the concentration for nucleation is much higher than that for growth. Therefore, in these systems, nucleation and growth are two separate processes.

In these reactions, the size of the inorganic core is a function of the time and the temperature. Especially, the growth time is a key parameter that determines

the size of nanocrystals. Longer growth time results in larger particles. More-over, higher temperatures support also larger particles since the energy required for Ostwald ripening decreases. Therefore, by tuning the growth time and the temperature, QDs having different sizes can be obtained.
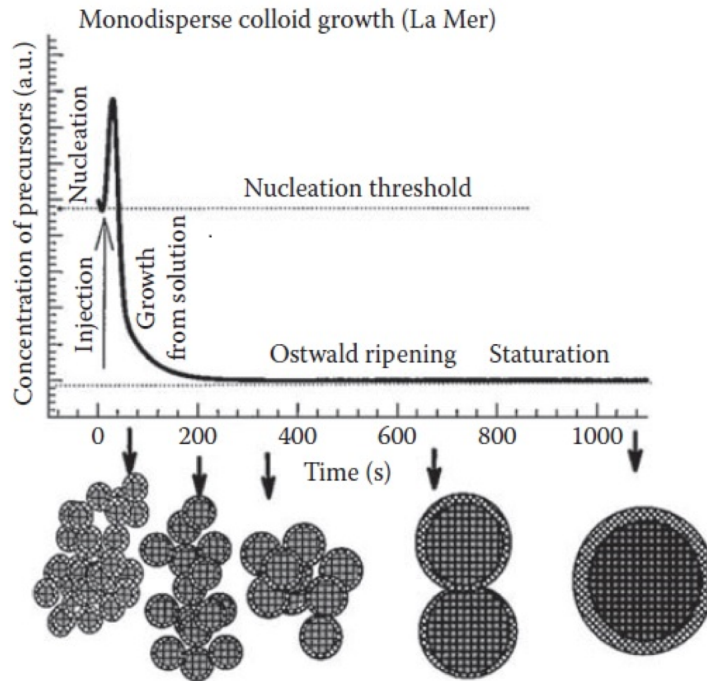
Figure 2.2: The nucleation and growth of NCs synthesis is modelled by La Mer and Dinegar model. Reprinted with permission from [1].

Ligands also play an important role in the chemical synthesis of nanocrystals. They bond to the core surface for different purposes. In the case of NCs, inorganic core should be surrounded by the ligand molecules to increase their solubility and stability in polar or nonpolar solvents and to neutralize their surface charge. Fatty acids like oleic acid and oleyamine are examples of widely used organic ligands. There are also inorganic ligands that are widely used to functionalize the surface of nanocrystals to increase electrical conductivity. For example, $Sn_2S_6^{4-}$ ligand capped CdSe QDs were demonstrated to increase the conductivity in transistors [32]. Although inorganic ligands improve the electrical properties, they might have a negative effect on the optical properties. Therefore, it is important to design NCs with an appropriate enclosure of ligands.

7

Comprehending the effects of all these parameters on the reaction kinetics and the properties of NCs has enabled to achieve different architectures other than quasi-0D QDs. Currently, NCs having different shapes can be synthesized with high monodispersivity and high quality.

2.3   Colloidal Quantum Wells

Colloidal quantum wells (CQWs) also commonly known as nanoplatelets (NPLs), are two-dimensional structures [13]. Exciton in these atomically-flat NPLs can freely move in lateral directions whereas it feels strong confinement in the thickness direction.As a schematic illustration, 4 monolayer (ML) thick CdSe NPL can be seen in Figure 2.3 (a). These NPLs consist of 4 layers of selenium atoms and 5 layers of cadmium atoms so that their surfaces are terminated by Cd atoms. Moreover, 4 ML and 5 ML CdSe NPL images obtained by high-angle annular dark field transmission electron microscopy (HAADF-TEM) can be seen in Figure 2.3(b) and 2.3(c). Since their lateral dimensions are larger than their exciton Bohr radius (5.6 nm for CdSe), NPLs show vertical confinement.

Typical absorption and emission profiles of 4 ML thick NPLs are presented in Figure 2.4. The first excitonic peak in the absorption spectrum at 510 nm corresponds to the heavy hole to the conduction band transition and the transition at 484 nm corresponds to the light hole to the conduction band. Their step-like absorption features are similar to epitaxial quantum wells, which have step-like density of states. As a consequence, NPLs are aptly named colloidal quantum wells [33]. Furthermore, the very sharp emission of NPLs is observed in their photoluminescence (PL) spectrum (Figure 2.4(b)). The full-width-half-maximum (FWHM) value of this emission is narrower than 10 nm, corresponding to ~ 35 meV, which is an indication of only homogenous broadening, lacking inhomogenous broadening.
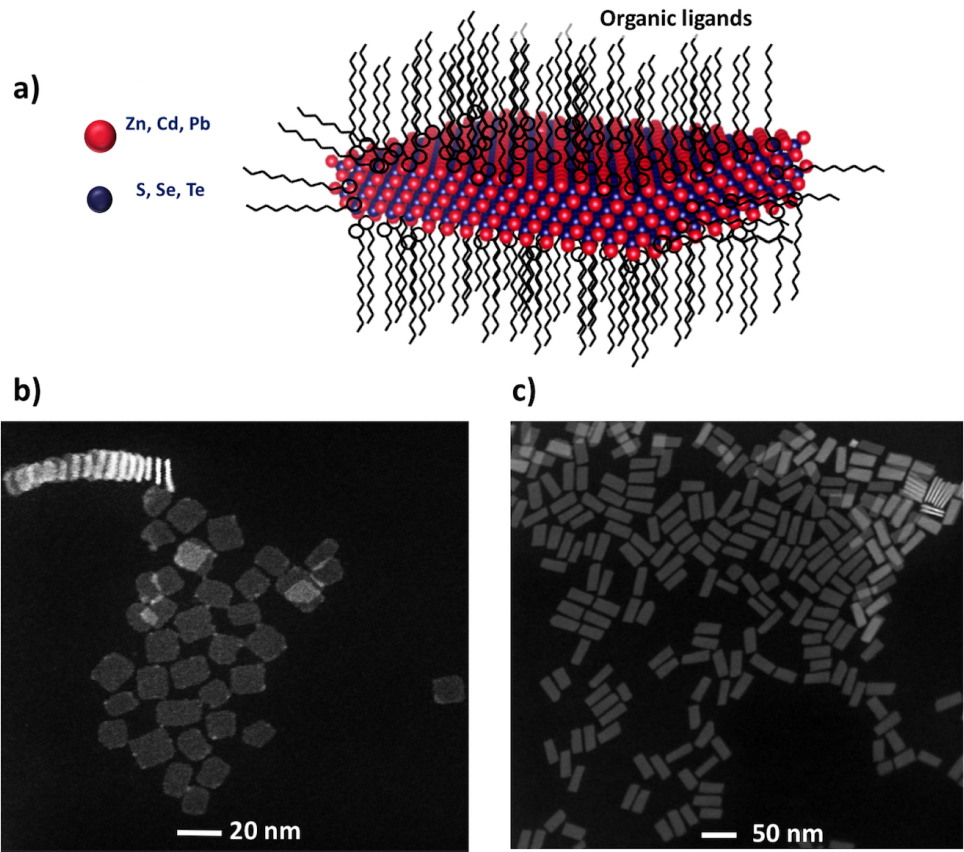
Figure 2.3: (a) Schematic representation of 4 ML CdSe NPLs, (b)HAADF-TEM image of 4 ML NPLs, and (c) HAADF-TEM image of 5 ML CdSe NPLs.

In Figure 2.5, absorption and emission spectra of NPLs having various thickness are presented. As it can be seen, their confinement stems from their vertical thicknesses regardless of their lateral dimensions as long as they are large enough. 4 ML thick CdSe NPLs have an emission peak centered at 513 nm. If the material is 3 ML thick (0.9 nm), the effective band gap energy increases so as the confinement energy, resulting in blue-shifted emission and absorption features. For increasing thickness, in the case of 5 ML thick (1.5 nm) NPLs, the band gap energy decreases [34] .

In addition to the core only structures, different heterostructures of NPLs can be synthesized. Without changing the thickness of the NPLs, the crown can be grown in the lateral direction. Furthermore, the top and bottom surfaces of NPLs can be coated with another type of semiconductor forming core/shell
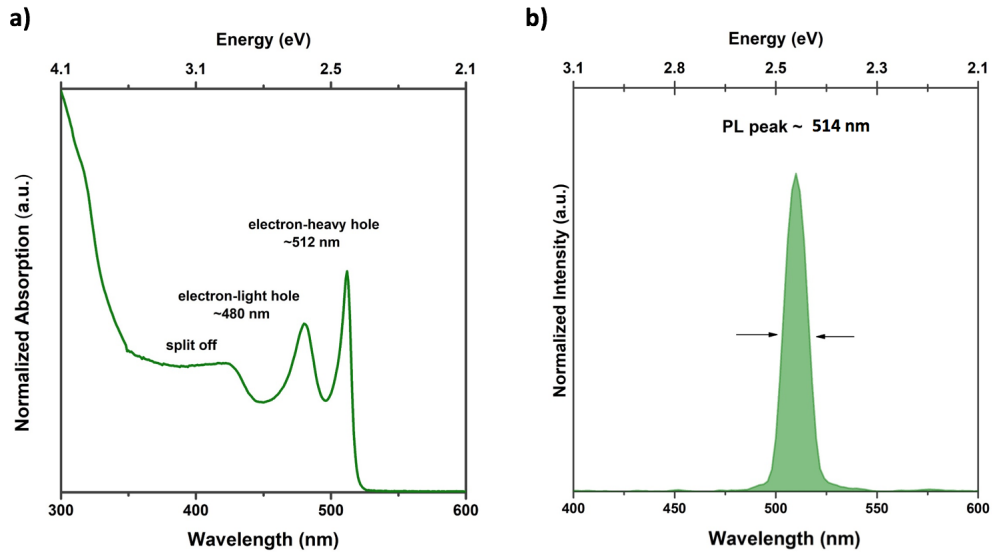
Figure 2.4: (a) Absorption and (b)PL spectra of 4 ML thick CdSe NPLs.

structures. By coating a shell or a crown, depending on the band alignment at the interface either Type-I, Type-II or Quasi Type-II electronic band structures can be obtained.

In Type-I electronic structures, electron and hole wave functions are confined in the same parts of the structure. CdSe/ZnS core/shell NPLs is a good example of this type of band structure [35] since ZnS has a higher band gap than CdSe, both electron and hole wave functions are strongly confined in the core and the tunneling is substantially suppressed. In Type-II band structure, electron and hole wavefunctions are localized in different parts of the structure, resulting in lower oscillator strength compared to Type-I electronic structure. CdSe/Cd$Se_{1-x}\ Te_x$ core/alloyed crown NPL is a good example of Type-II band alignment. CdSe/CdS core/crown NPL is an example of quasi Type-II structures where partial separation of electron-hole wave functions occur. Since the conduction band is formed by cation's unoccupied electrons which is Cd 5s electrons in this case, conduction band offsets of CdSe and CdS are close to each other resulting in delocalization of electron wave function to whole structure.
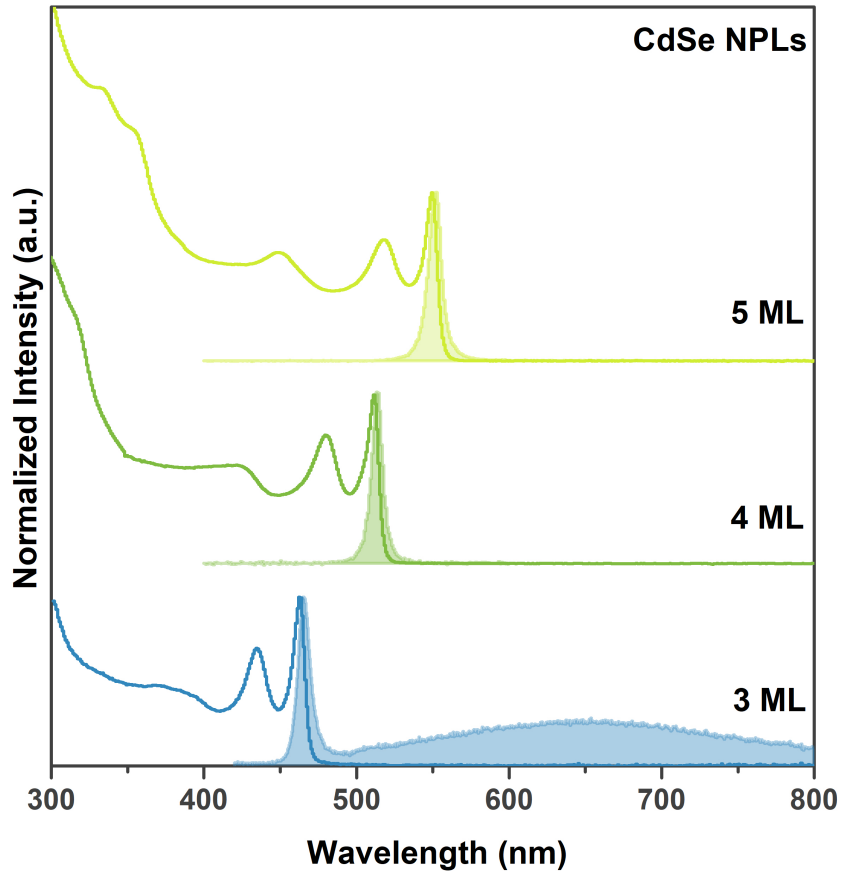
Figure 2.5: Absorption and PL spectra of NPLs having various thickness (in MLs).

By designing the electronic band structure of NPLs, optical properties can be changed. For example, the photoluminescence quantum efficiency (PL-QY) of CdSe NPLs can be increased from 20-25% to 70% by growing CdS crown [36]. Another example could be the coating the top and bottom surfaces of core CdSe NPLs with CdS by colloidal atomic layer deposition (c-ALD) technique [37],[38]. With this technique, atoms can be grown on the surface of NPLs layer by layer in a very controlled manner. By passivating surfaces of CdSe NPLs with CdS, emission properties can be tuned in the red region of UV-Vis spectrum. Moreover, passivating the top walls of the NPLs provides suppression of Auger

recombination resulting in improved photophysical properties of NPLs.

Core only NPL

Core/crown NPL
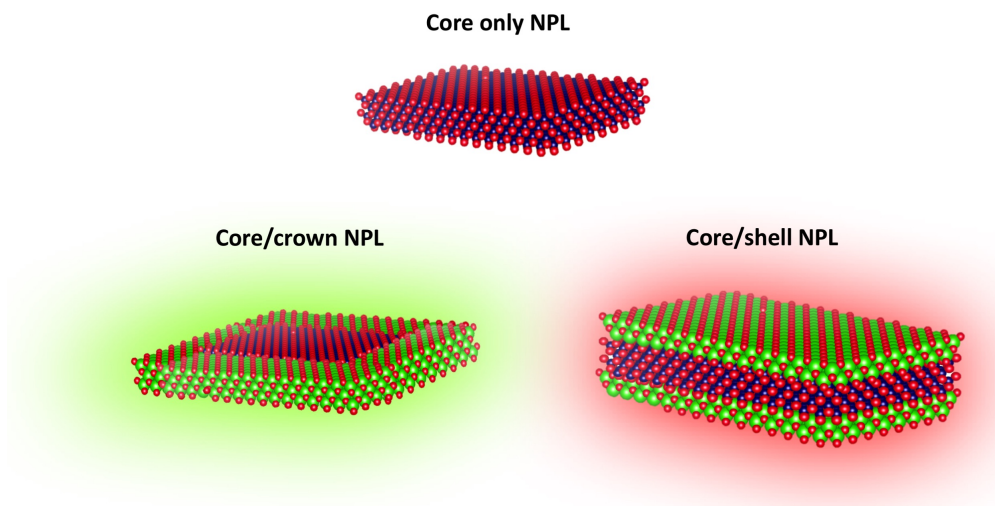
Core/shell NPL

Figure 2.6: Schematic representation of the core-only, core/crown and core/shell NPLs.

Chapter 3

Characterization Methods of Colloidal Quantum Wells

In this chapter, the characterization approaches of the colloidal quantum wells by using different tools are discussed. By using these techniques, one can understand the physical, chemical and optical properties of the synthesized nanoplatelets.

3.1 Optical Characterization Techniques

Absorption and photoluminescence (PL) spectroscopies are the most widely used characterization techniques that help to measure the steady-state excitonic properties. In our works, optical characterizations have been performed using UV-Vis and UV-Vis-NIR spectrometers (Cary 100 and Cary 5000) for absorption measurements and fluorescence spectrometer (Cary Eclipse) for PL measurements. Moreover, time-resolved fluorescence (TRF) spectroscopy is a powerful technique to study emission kinetics of an NPL structure. In the experiments, TRF measurements are carried out by Pico Quant FluoTime 200 spectrometer.

3.1.1 Steady-State Absorption Spectroscopy

When incident light interacts with the material, it can be either absorbed, transmitted, reflected or scattered. Simply, the absorption spectrum of the material shows which portion of the incident light is absorbed by the material. Our colloidal nanocrystals absorb part of the UV-Vis region of the electromagnetic spectrum. According to our experimental setup, a cuvette filled with nanoplatelets dissolved in a suitable solvent is placed inside the instrument and scanned all the wavelengths from 200 to 1100 nm covering the UV-Vis region. Depending on the energy of the incoming photon, a certain portion of the light might be absorbed, some portion might be transmitted or reflected and absorption can be expressed by using Beer-Lambert Law

$$A = \epsilon \times l \times C \tag{3.1}$$

where A is the absorbance (unitless), ϵ is the molar extinction coefficient (L/mol-cm) which is the material's property, l is the optical path length (width of the cuvette, cm), and C is the concentration of our nanoplatelets inside the solvent (mol/L). As an exemplary case, simple absorption spectrum of 5 ML thick core CdSe NPLs is presented in Figure 3.1. In the absorption spectrum, excitonic transitions from the valence band to the conduction band can be seen. Conduction band is formed by Cd 5s orbital and valence band is formed by Se 4p orbitals. Due to the degeneracy of p orbitals, there are 3 bands in the valence band: heavy hole, light hole, and the split off bands. The first and second excitonic transitions correspond to heavy-hole to conduction band and light-hole to the conduction band transitions, respectively, and the third peak in the spectrum is called split-off band. The peak positions of these bands in NPLs strongly depend on thickness and, for the certain thickness, these peaks always locate at the same wavelength.
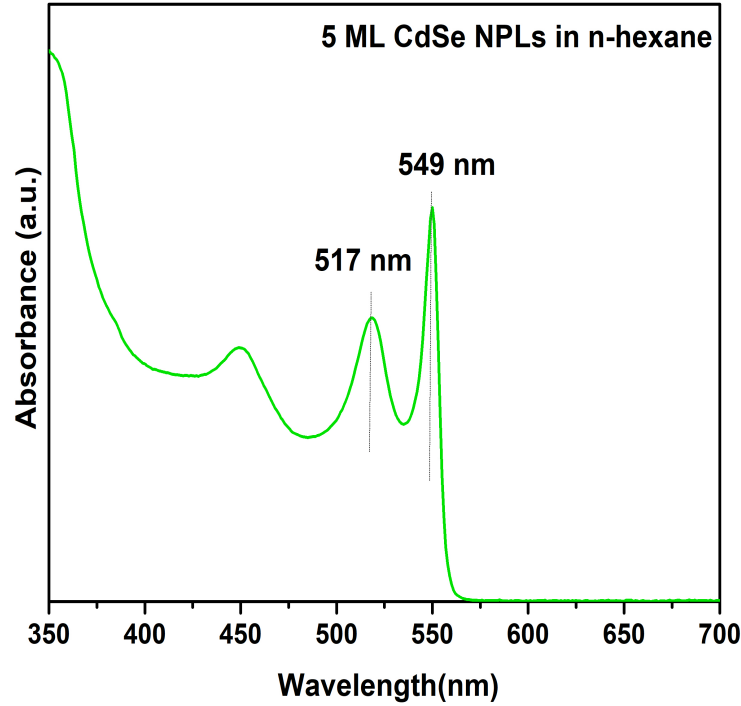
Figure 3.1: Absorption spectrum of 5 ML thick CdSe core NPLs. Heavy-hole and light hole to conduction band transitions can be seen.

Additionally, increase in the thickness of the NPLs results in decrease in the confinement energy so that spectrum red-shifts to the lower photon energies. In Figure 2.5, the absorption spectra of 3 ML, 4 ML, and 5 ML thick NPLs can be seen. From the absorption spectra, the 1st excitonic peaks of 3 ML ($\sim$ 0.9 nm), 4 ML ($\sim$ 1.2 nm), and 5 ML ($\sim$ 1.5 nm) thick NPLs are located at 460, 513 and 550 nm regardless of their lateral dimensions. Therefore, thanks to strong dependence of their optical properties over their thickness, the absorption spectroscopy helps to determine the thicknesses of the as-synthesized NPLs [34].
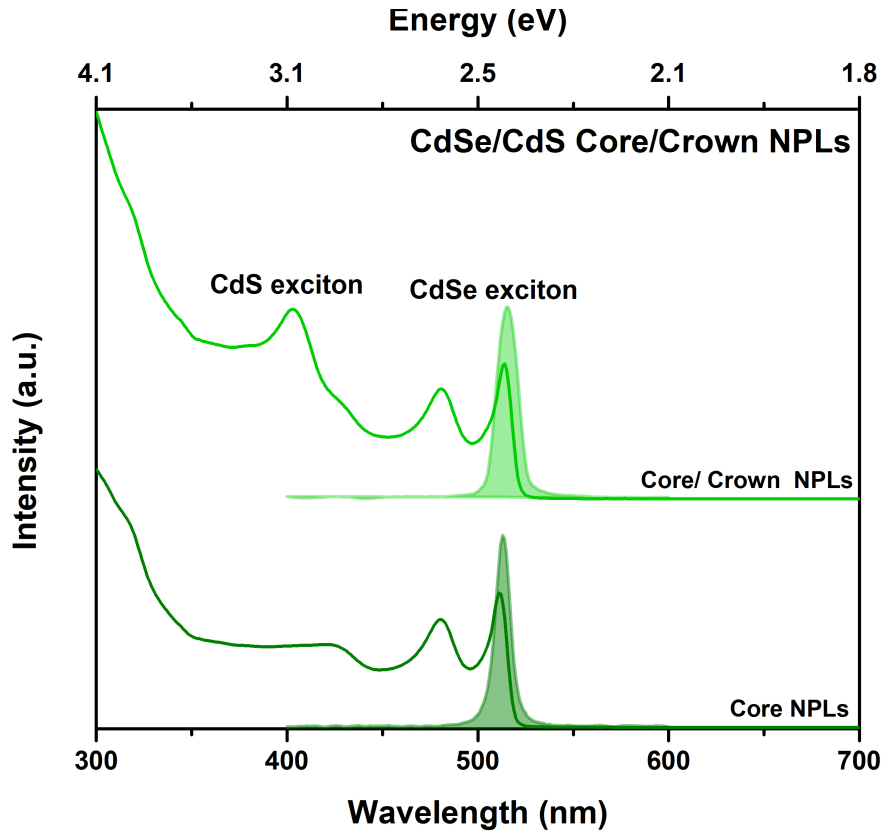
Figure 3.2: Absorption and PL spectra of 4 ML CdSe core-only and CdSe/CdS core/crown NPLs.

Moreover, the absorption spectroscopy can be used to verify the formation of heterostructures of NPLs. For example, in 4 ML CdSe/CdS core/crown NPLs, the formation of CdS can be confirmed by taking the absorption spectrum. As shown in Figure 3.2, different than the CdSe core spectrum, at $\sim$ 405 nm, there is a peak formation that occurs as a result of CdS. Since the thickness does not change in core/crown structures, excitonic features of the cores are preserved at the same spectral position. Similarly, in CdSe/CdS core/shell heterostructures, with the increasing number of shell layers, electron and hole wave functions relax, resulting in red-shifting in the excitonic features. Therefore, the addition of number of layers can be estimated by the absorption spectrum (Figure 3.3).
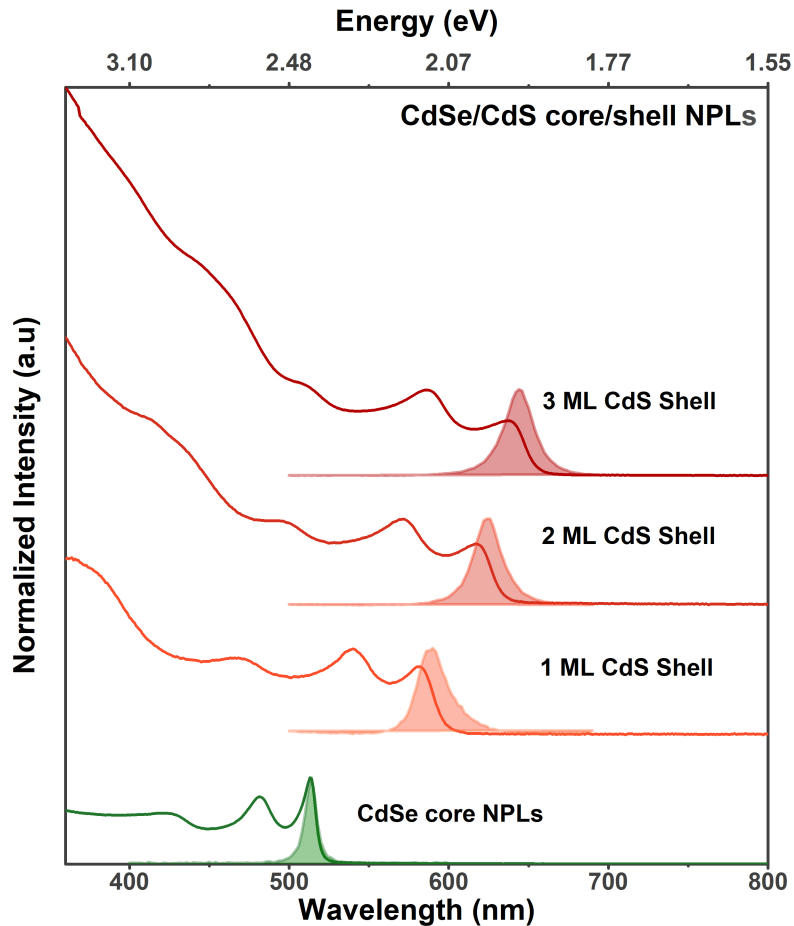
Figure 3.3: Absorption and PL spectra of 4 ML CdSe core-only and CdSe/CdS core/shell NPLs having different monolayers.

3.1.2 Steady-State Photoluminescence Spectroscopy

Fluorescence spectroscopy basically consists of two different monochromators (one for emission and one for excitation), mirrors, a light source, and a detector. The light source provides a broadband spectrum and by using a monochromator a narrow spectrum at a desired wavelength can be obtained. When a sample is excited, photons are absorbed by the sample if the excitation spectrum is in the absorption band of the sample. This leads to the generation of an excited electron and hole, which are physically in the same location and are attracted one to another by coulombic interaction. This photogenerated electron-hole pair
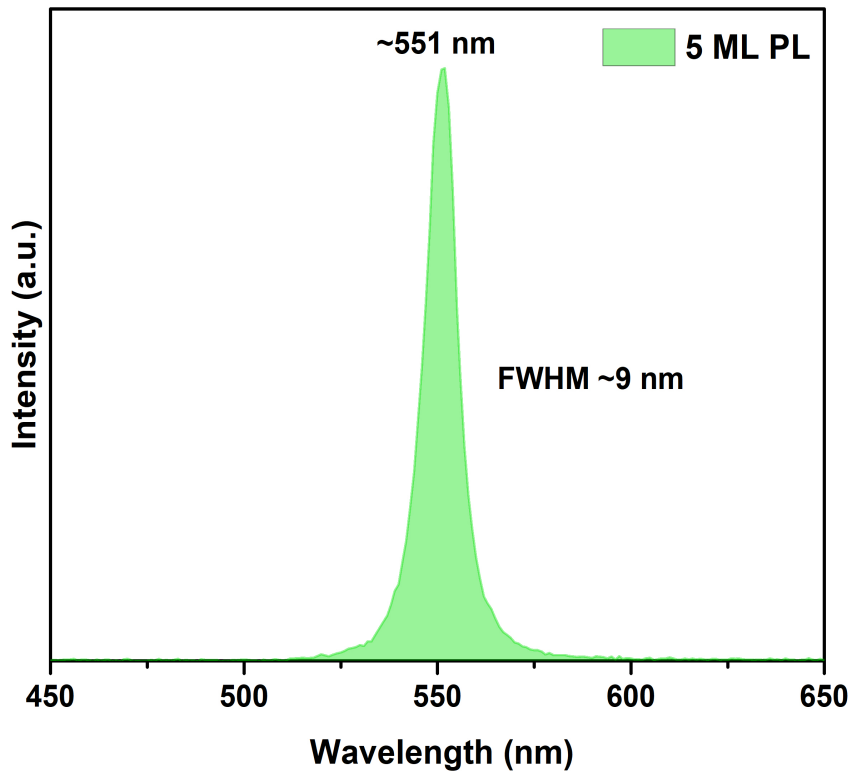
Figure 3.4: PL spectrum of 5 ML thick NPLs.

is an exciton. Then, the recombination of this exciton gives rise to the emission of a photon. This emission is collected by another monochromator, which scans the UV-Vis spectrum, and subsequently detected by the detector, converting the collected photons into an electrical signal.

In Figure 3.4, the emission spectrum of 5 ML thick NPLs dissolved in hexane can be seen. At room temperature, the PL emission has a peak position centered at 551 nm with a FWHM narrower than 10 nm. By using the fluorescence spectroscopy, similar to the absorption, different NPL thicknesses can be identified. As it can be seen from Figure 2.5, 3 ML thick CdSe NPLs have an emission peak centered at ~ 465 nm, whereas it is ~ 514 nm for a 4 ML NPL and ~ 553 nm for a 5 ML NPL, respectively. Therefore, the fluorescence spectroscopy is an important instrument to determine the thickness of the synthesized NPLs.

3.1.3 Photoluminescence Excitation Spectroscopy

Besides the absorption and PL measurements, another important technique is the photoluminescence excitation (PLE) spectroscopy. It is quite similar to the PL spectroscopy; however, in this case, the emission monochromator is fixed at the defined wavelength, which is typically in the emission band and is the emission peak wavelength of the material and the excitation monochromator scans the spectral range for excitation. Then, intensity of the collected emission is recorded as a function of the excitation wavelengths. PLE spectrum is taken to understand the origin of the emission. Therefore, the PLE spectrum should resemble the absorption spectrum of the NCs.
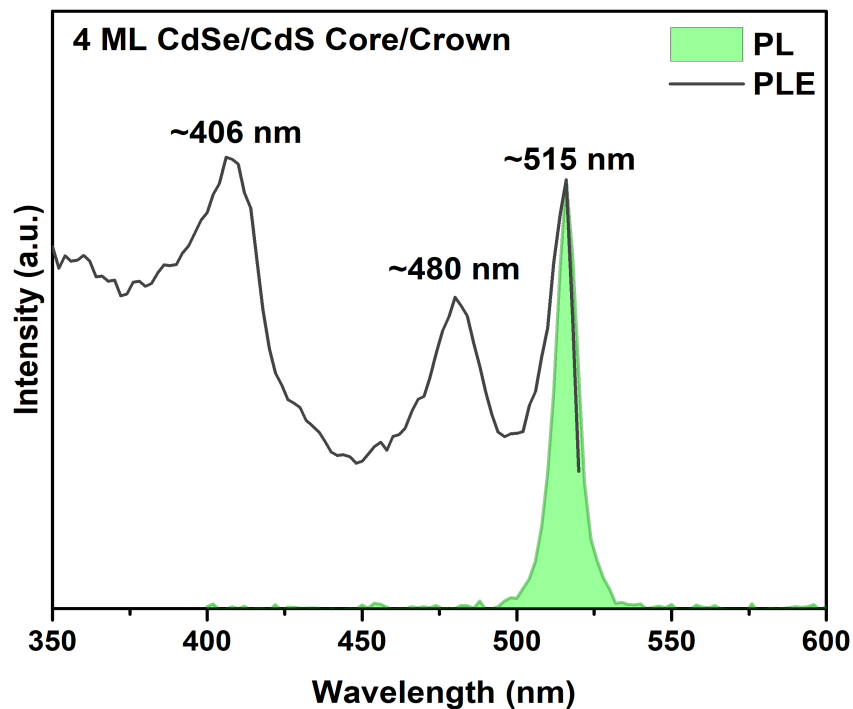
Figure 3.5: PLE spectrum of 4 ML CdSe/CdS core/crown NPLs.

In Figure 3.5, the PLE spectrum of 4 ML thick CdSe/CdS core/crown NPLs is shown as an example. This PLE spectrum was taken at the peak position of the emission and, as it can be noticed, this spectrum is very similar to the

absorption spectrum (Figure 2.7). From the spectrum here, it can be concluded that there is no seperate CdS nucleation and CdS only grew around the periphery of the starting CdSe core. In this thesis, we commonly used PLE spectroscopy to understand the quality of the synthesis.

3.1.4 Photoluminescence Quantum Yield Measurements

Photoluminescence quantum yield (PL-QY) is an important performance metric that quantifies the emisison efficiency of the nanocrystals. It is the ratio of the number of emitted photons to the number of absorbed photons. In the literature, PL-QY can be measured in two different methods: the absolute fluorescence quantum yield and relative fluorescence quantum yield. For the relative PL-QY, a reference material with a well-known quantum yield (mostly dye molecules) is used to compare with an unknown sample. Concentration of the materials are adjusted to have the same absorbance values and then PL from these two materials is measured by a fluorescence spectrometer under the same conditions (excitation wavelength, excitation and emission slit sizes). By comparing the areas under the PL curves (number of photons emitted), the QY of the unknown sample can be calculated.

In absolute measurements, the sample's QY is calculated directly from its absorption and emission. A cuvette filled with the sample is placed inside a integrating sphere, which contains a highly reflective coating. Then, four different spectra are taken to calculate the QY: i) one spectrum is collected when there is no sample inside, ii) another spectrum is collected when the sample is excited directly by the light source iii) another is collected when the sample is excited indirectly with scattered light and lastly iv) the response of the spectrometer is collected when there is no light in the integrating sphere. By these measurements, the quantum yield can be calculated according to de Mello method [39], which basically calculates the ratio of emitted photons to the absorbed photons.
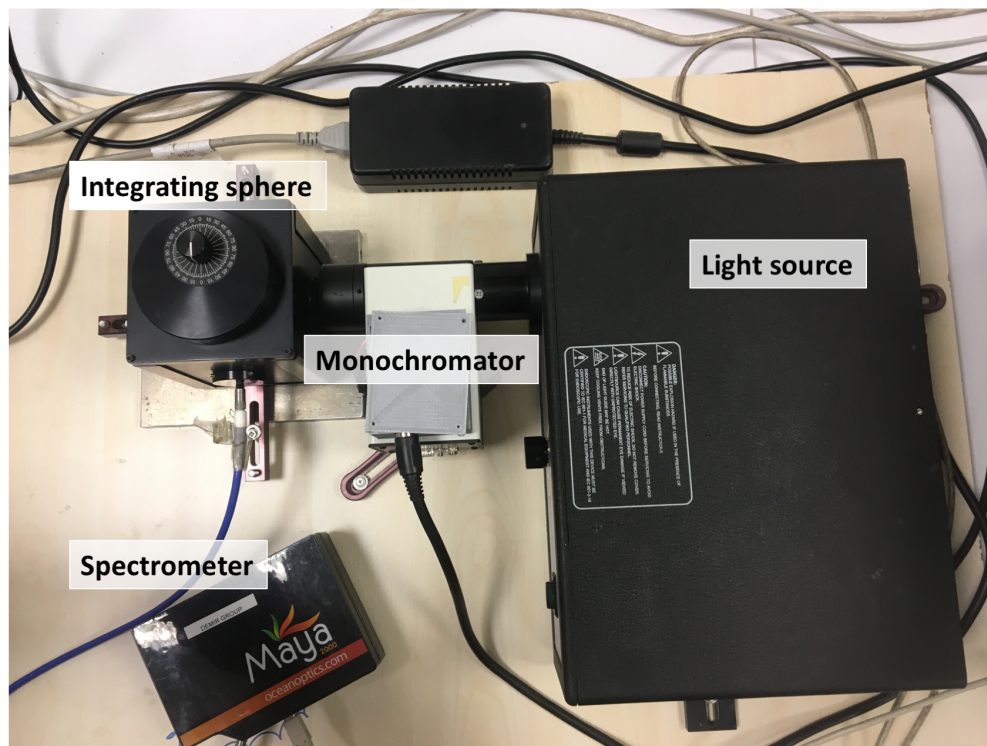
Figure 3.6: PL-QY setup in our laboratory. Four basic components can be seen: a light source, a monochromator, an integrating sphere and a spectrometer.

3.1.5 Time-Resolved Fluorescence Spectroscopy

Time-resolved fluorescence spectroscopy (TRF) is a useful technique to study excited state dynamics of fluorescent materials. We studied time-resolved fluorescence of the NPLs with a FluoTime 300 time-resolved spectrometer and a PicoHarp 200 time-correlated single photon counting (TCSPC) unit. The setup consists of a laser at a specific wavelength (375 nm), a monochromator, a photomultiplier tube (PMT), and a laser control unit. In principal, samples are excited by a pulsed laser and then the emitted photons from the sample are detected by a PMT at a selected wavelength each with a certain time of light following the pulsed excitation. Inside the PMT, the photons are converted into electrons and the current is directly proportional to the intensity of the light. At the end, the detected photons are count as a function of the time. These photon counts from many excitation events are consolidated to compose a decay curve over time. By

studying the kinetics of this decay, one can obtain information on the sample's photoluminescence lifetime, which is an important characteristic of nanocrystals.

As an example, the fluorescence decay curves of the CdSe core-only, the CdSe/CdS core/crown and the CdSe/CdS core/shell NPLs in solution are presented in Figure 3.7.These NPLs were dissolved in suitable solvents (e.g., n-hexane, toluene) and they were excited by our pulsed laser at 375 nm. To analyze these PL decay curves of the samples,they were fitted by multi-exponential functions convoluted with impulse response function (white curves in Figure 3.7).
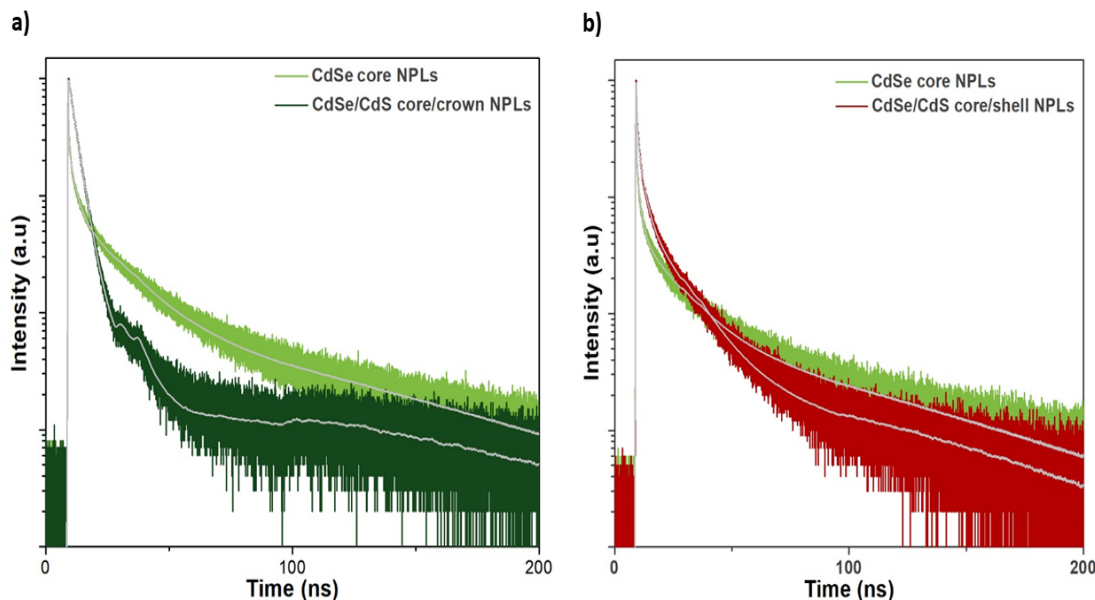
Figure 3.7: Time-resolved fluorescence decay curves of 4 ML CdSe core-only and (a) CdSe/CdS core/crown, and (b) CdSe/CdS core/shell NPLs.

3.2   Structural Characterization Techniques

Optical properties of semiconductor materials are determined by their electronic structure. By using transmission electron microscopy, shape, size, structure and elemental composition of a nanoplatelet can be determined. Chemical composition of materials can be identified by X-ray photoelectron spectroscopy. Here, we explain these two methods to characterize our structural NPL properties.

3.2.1 Transmission Electron Microscopy

Transmission electron microscopy (TEM) is a quite essential technique in the field of nanophotonics in general and for studying nanocrystals in particular. Shape, size, structure, and chemical composition of the nanocrystals can be determined by TEM.
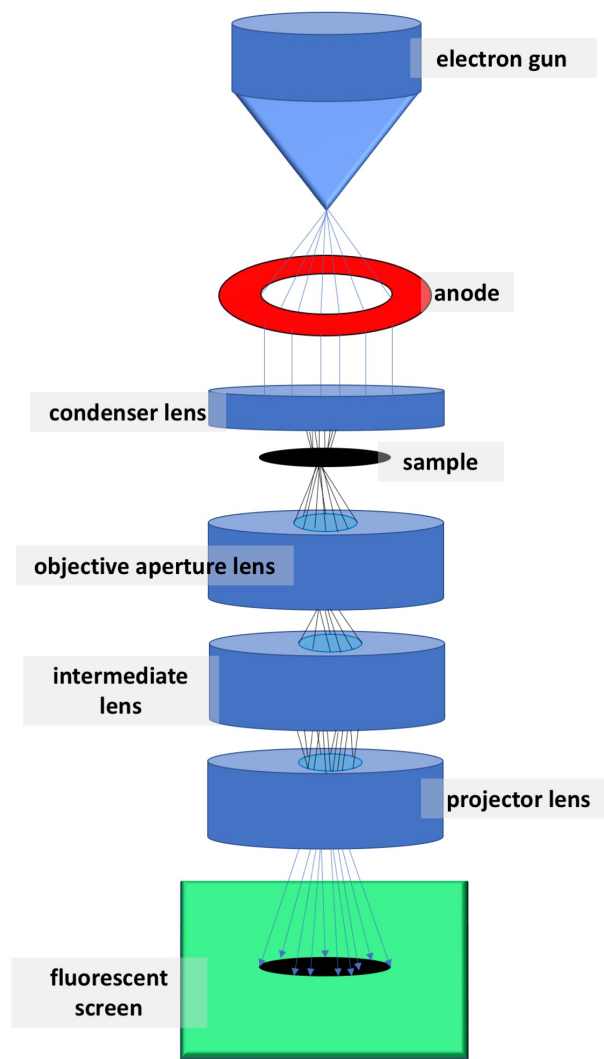
Figure 3.8: Schematic representation of transmission electron microscope.

Similar to light microscopy, electron microscopy works with the same principles. However, the sources used in electron microscopes are different. Electron microscopy uses electrons instead of light. As it can be seen in the basic schematics of TEM in Figure 3.8, electrons are created by an electron gun (LaB_6 or thermionic) and accelerated under high voltage typically between 100-300 kV. The electron beam is then focused by condenser lenses, which are made of magnetic coils. Then, electrons hit the surface of a specimen, and are scattered. With the help of the objective lenses, these scattered electrons are collected and an image is formed. The electron microscope is operated under high-vacuum atmosphere since air could absorb the electrons. The typical resolution of TEM is 0.2-0.5 nm, which is the common distance between two atoms in the crystal [40].

In this thesis, we most commonly used TEM to characterize the shape of the synthesized NPLs. Since our nanocrystals are typically suspended in nonpolar solvent (hexane, toluene, etc.), the sample preparation is relatively simple. Our NPL sample preparationfor TEM is as follows. A diluted solution of NPLs is cleaned few times to remove excess ligands which otherwise causes charging effect under the microscope. After cleaning steps, 7 μL of this cleaned and diluted solution is dropped on a copper mesh grid and waited for the evaporation of its nonpolar solvent. For further drying, the copper grid is kept under vacuum before examining under the TEM.

Our NPLs typically have lateral sizes on the order of 10-50 nm and their thickness is between 1-2 nm, which gives low intensity to examine them under transmission mode of TEM. For this reason, we used high-angle annular dark field scanning transmission electron microscopy (HAADF-STEM) to image the size and shape of our nanocrystals at high contrast levels. In this mode, transmitted fraction of the electron beam is collected by HAADF detector to form an image. As an example, 4 ML CdSe/Cd$Se_{0.95}Te_{0.05}$ core/crown NPLs can be seen in Figure 3.6. Their lateral dimensions are 15 nm $\times$ 35 nm, and also the thickness can be calculated from stacked NPLs,which is 1.2 nm in this case.
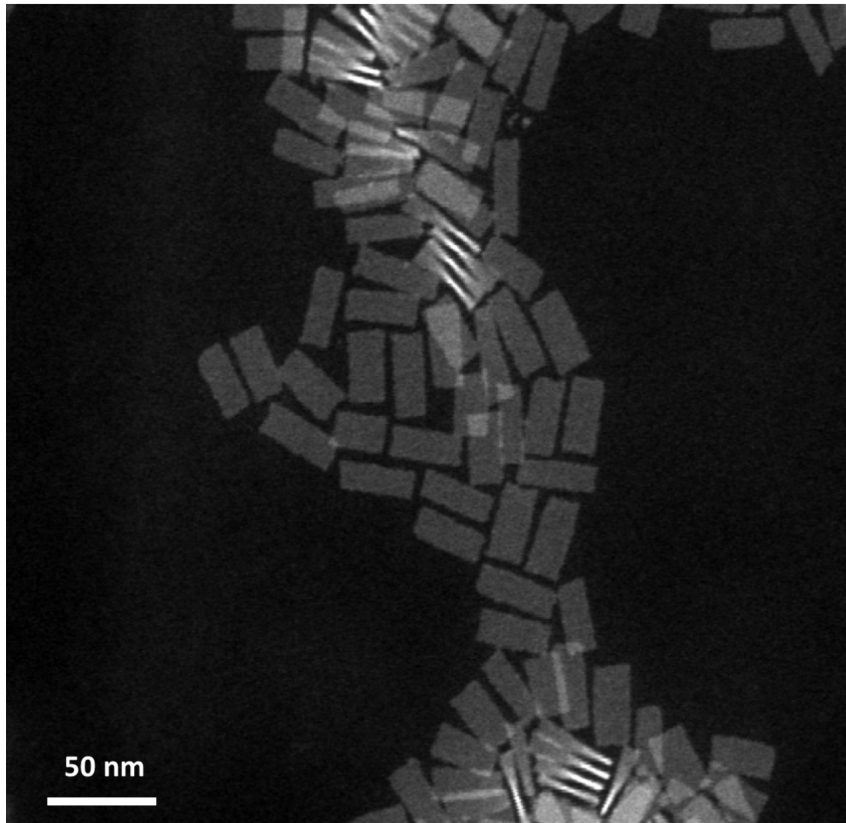
Figure 3.9: HAADF-TEM image of CdSe/Cd$Se_{0.95}Te_{0.05}$ core/cown Type II NPLs.

3.2.2 X-Ray Photoelectron Spectroscopy

X-ray photoelectron spectroscopy (XPS) is a very useful technique among electron spectroscopies for analyzing the surface of various material types. Basically in XPS, created X-rays are sent to a sample and then the kinetic energy of electrons ejected from the sample is analyzed based on the relation:

$$KE = h\nu - E_b - \phi \tag{3.2}$$

Here KE is the kinetic energy of the emitted electrons analyzed by the detector, $h\nu$ is the energy of the X-rays sent to the sample, E_b is the binding energy of the photoelectrons emitted from the sample, and ϕ the is the spectrometer work

function. Generally, MgK (1253.6 eV) or AlK (1486.6 eV) is used as an ordinary X-ray source so that the source energy is known [2]. Moreover, the work function of the spectrometer (instrument) is a constant parameter for a specific instrument and the kinetic energy of the electron is also known by the detector so that the binding energy of the ejected electrons can be calculated. The binding energy is defined as the energy required to eject an electron from a particular shell of an atom in the material. It is a function of the electron-electron interactions, the distance between the core electrons and the nuclei, and the number of protons present in the nuclei.
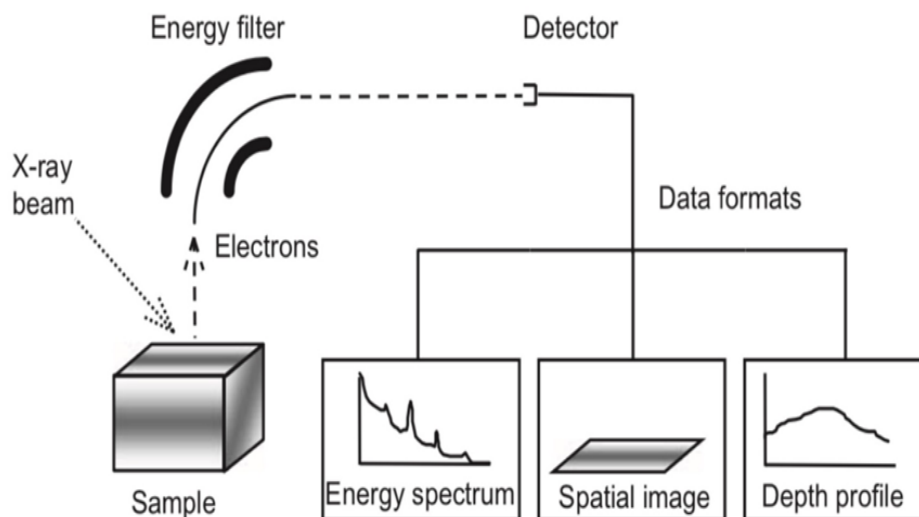
Figure 3.10: Schematic representation of XPS. Reprinted with permission from [2].

In our studies, wencommonly used XPS for the quantification of the elemental composition of our synthesized materials. In this thesis, we calculated the ratio of selenium to tellurium in $CdSe_{1-x}Te_x$ alloyed NPLs. Furthermore, the presence of sulfur in $CdSe/CdSe_{1-x}Te_x/CdS$ core/crown/crown NPLs, was determined using XPS.

Chapter 4

Colloidal Synthesis and Characterization of Aspect Ratio Dependent Core Quantum Wells

4.1 Motivation

Colloidal quantum wells, or nanoplatelets, are atomically flat two-dimensional materials. Their lateral dimensions are typically larger than their exciton Bohr radius and their strong confinement is the result of their vertical thickness commonly of few monolayers (3 ML, 4 ML, 5 ML). Since their discovery [13], these semiconductor NPLs have been in the spotlight because of their promising optical properties [41]. They feature very narrow luminescence spectra (~ 10 nm) thanks to their pure magic-sized vertical confinement [34]. Their step-like sharp absorption profile, their giant oscillator strength, their extremely large linear and nonlinear absorption cross-sections are among their attractive properties [42]. All these properties make these materials excellent candidates towards designing high-performance colloidal structures and devices [43] [44] [45].

NPLs have become one of forefronts of the colloidal nanoscience since their discovery. Even though these NPLs can be synthesized in a well-controlled synthesis procedure, the underlying mechanisms behind their formation are still being studied. Lately, Riedinger et al. proposed a theory based on the growth instability that results in NPL formation [46]. On the other hand, Chen et al. suggested a different mechanism on their formation based on intra-particle ripening [47].

square   **rectangular**   **rod-like**
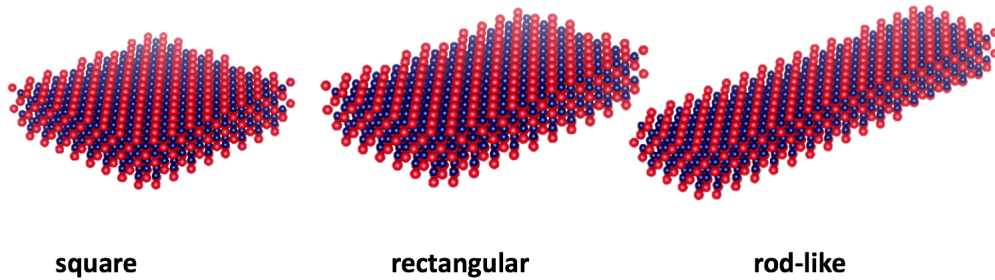
Figure 4.1: Illustration of different nanoplatelet shapes with different aspect ratios.

While various research groups have been working on understanding the mechanisms behind their formation, our group has looked into the effect of their lateral shape observed on some of their properties. The optical properties of these NPLs moainly depend on their vertical thickness, which is the only tight dimension that is smaller than its exciton Bohr radius. However, their lateral size is another important parameter that affects their properties. We previously showed that larger core NPLs have lower PL-QY due to increased surface defects, which significantly changes their spontaneous and amplified spontaneous emission [48]. Lately, Li et al. suggested a model for optical gain in core-only NPLs using femtosecond transient absorption spectroscopy [49]. They reported that the optical gain threshold is not a function of the NPL lateral area, whereas the saturation gain amplitude is. Both of these previous studies give an insight that there is an effect of the lateral size on the NPL optical behavior. However, these previous studies both used NPLs having lateral lengths and widths larger than exciton Bohr radius of the material.

In this thesis work, we synthesized rod-like, rectangular and square 4 ML

thick CdSe core-only NPLs, while managing to keep their lateral area constant. In the rod-like NPLs, the width of the NPLs is slightly smaller than exciton Bohr radius of CdSe resulting in slightly blue-shifted emission and absorption features. Furthermore, we studied the effect of the aspect ratio of their lateral dimensions on the amplified spontaneous emission process, again keeping the lateral area constant.

4.2 Experimental

4.2.1 Chemicals

Chemicals and solvents that are used in the synthesis include cadmium nitrate tetrahydrate $[Cd((NO_3)_2).4H_2O]$ (99.999% trace metals basis), cadmium acetate anhydrous $[Cd(Ac)_2]$, cadmium acetate dihydrate $[Cd(Ac)_2.2H_2O]$ ($\geq$ 98%), cadmium acetate monohydrate $[Cd(Ac)_1.2H_2O]$, sodium myristatic acid ($\geq$ 99%), 1-octadecene (technical-grade) (ODE), elemental selenium (Se) (99.998% trace metals basis), technical-grade oleic acid (OA) (90%). Hexane, ethanol, methanol were purchased from Sigma Aldrich.

4.2.2 Preparation of Precursors

In a typical cadmium myristate synthesis, 1.23 g of $[Cd((NO_3)_2).4H_2O]$ was dissolved in 40 mL of methanol and 6.26 g of sodium myristate was dissolved in 250 mL of methanol by continuous stirring. After 2 hours of stirring for dissolution, both solutions were mixed and stirred $\sim$ 2 more hours. Then, the white bulky precipitate of cadmium myristate was washed and cleaned with methanol by using Erlenmeyer flask. For better drying, the bulky precipitate was kept at the vacuum chamber for $\sim$ 24 hours.

4.2.3   Colloidal Synthesis of Core Quantum Wells

4 ML thick CdSe NPLs were synthesized by the following standard recipe from the literature [11]. In a three-neck 100 mL flask, 340 mg of cadmium myristate, 24 mg Se and 30 mL of ODE were loaded. With the help of a magnetic stirrer, the solution was degassed and mixed under vacuum at $90°C$ around 1 hour. During this procedure, vacuum pressure should be less than 1 mbar. The reason for degassing is to remove undesired solvents. Then, under an inert atmosphere (commonly argon flow), the temperature of the solution was set to $240°C$. When the temperature of the solution reached $195°C$, cadmium acetate precursor was added. After 9 min growth at $240°C$, 1 mL of OA was injected and the solution was cooled to room temperature by water quenching. When the solution temperature approached the room temperature (RT), 5 mL of hexane was injected for the better dissolution of NPLs. For square NPLs we used 120 mg of $Cd(Ac)_2.2H_2O$. For rectangular like NPLs, we used 90-110 mg of $Cd(Ac)_2.H_2O$ and for rod-like NPLs, we used 90-100 mg of $Cd(Ac)_2$.

In the purification step, NPLs were centrifuged at 6,000 rpm around 6 min. The first precipitate was redissolved in hexane and the supernatant was centrifuged with the addition of ethanol at 6,000 rpm. Since NPLs were capped with oleic acid, adding antisolvent (which is ethanol in this case) helps them to precipitate. The second precipitate was also dissolved in hexane. Then they were mixed and centrifuged at 10,000 rpm for 15 minutes. Finally, the supernatant was kept in a glass vial and stored in the fridge. All these steps help us to separate undesired reaction products including QDs, and 3 ML and 5 ML NPLs.

The water combined with cadmium acetate has a crucial effect determining the shape of the NPL [50]. Anhydrous acetate addition results in higher aspect ratio NPLs, whereas water addition results in more square shapes. Therefore, to obtain square shapes, dihydrous acetate was used. Moreover, rectangular shape NPLs were obtained by monohydrous acetate and, for rod-like NPLs, anhydrous acetate was used.
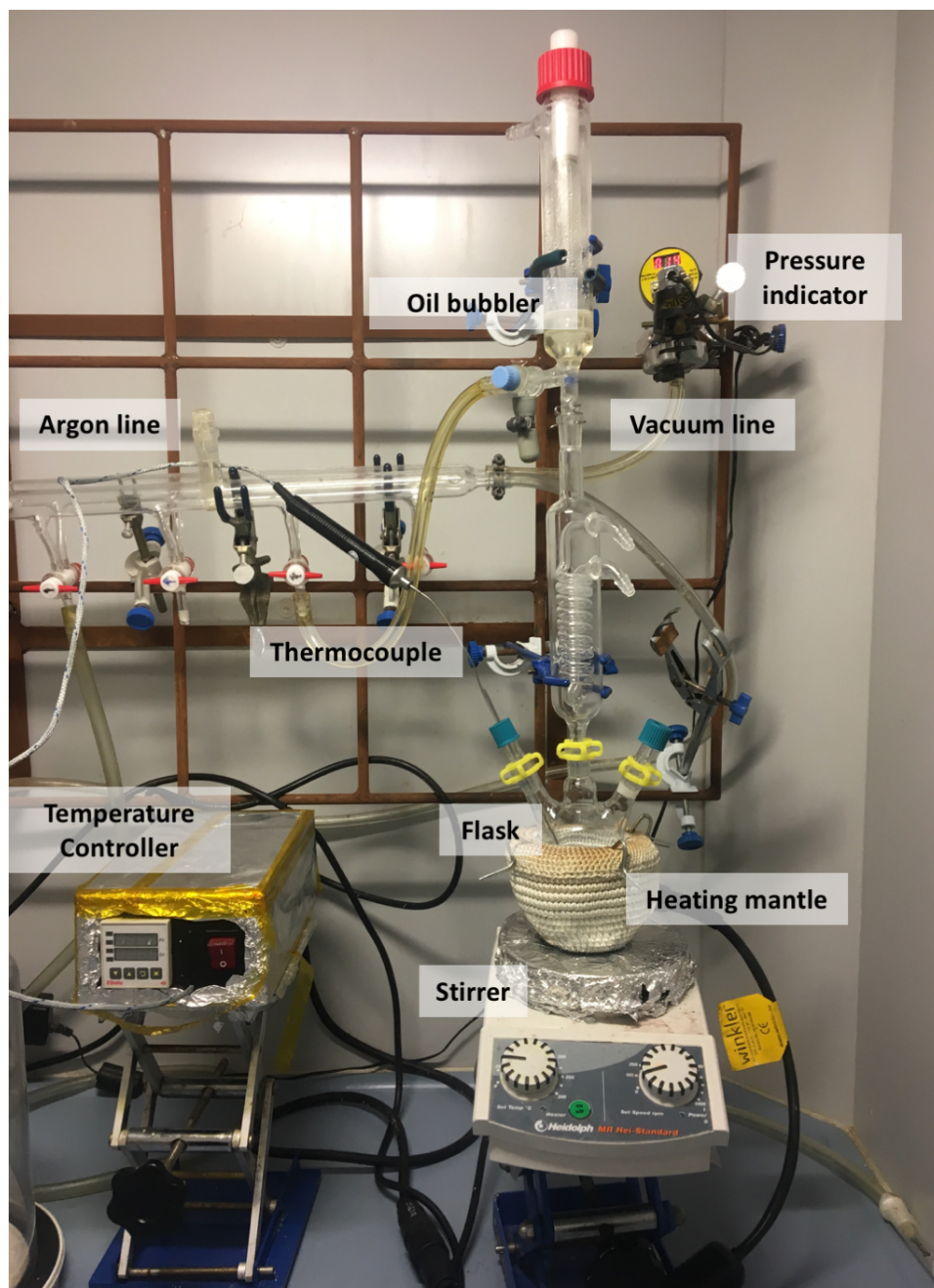
Figure 4.2: Photograph of Schlenk's line in our laboratory. This is a typical setup used for colloidal synthesis.

4.3 Results and Discussion

Amount of water chemically combined to acetate affects the shape of the core nanoplatelets. Moreover, the amount of acetate precursor added also plays a role to determine the lateral size of the NPLs. Therefore, by varying the quantity of acetate, the lateral size of the NPL can be altered. In this thesis, our purpose was to keep the surface area of the NPLs more or less the same while increasing their aspect ratio. Consequently, among different sizes of the square, rectangular and rod-like shapes, NPLs having the same lateral area were selected to further characterize and analyze.

4.3.1 Structural Chracterization

Following the synthesis of size-varied core NPLs, their shapes are characterized by transmission electron microscopy (TEM). In Figure 4.3, the square (a), the rectangular (b) and the rod-like (c) NPL images are given. They are highly monodisperse and their thickness can be seen from the stacked-NPLs. After imaging NPLs, we measured their average lateral sizes. The square NPLs have a 14.3 ± 1.8 nm width and a 17.1 ± 2.0 nm length. Both of side lengths surpass the exciton Bohr radius of CdSe, which is ~ 5.6 nm. Therefore, no lateral confinement could be observed. The rectangular NPLs have a width of 9.1 ± 3.1 nm and a length of 26.1 ± 2.0 nm. In the rod-like NPLs, the width varies between 3.7 to 6.0 nm having an average of ~ 5.3 nm and the long dimension lies between 35 nm to 45 nm having an average of 40.7 nm. Since the width of the rod-like NPLs is comparable with the exciton Bohr radius of CdSe, one would expect additional confinement.
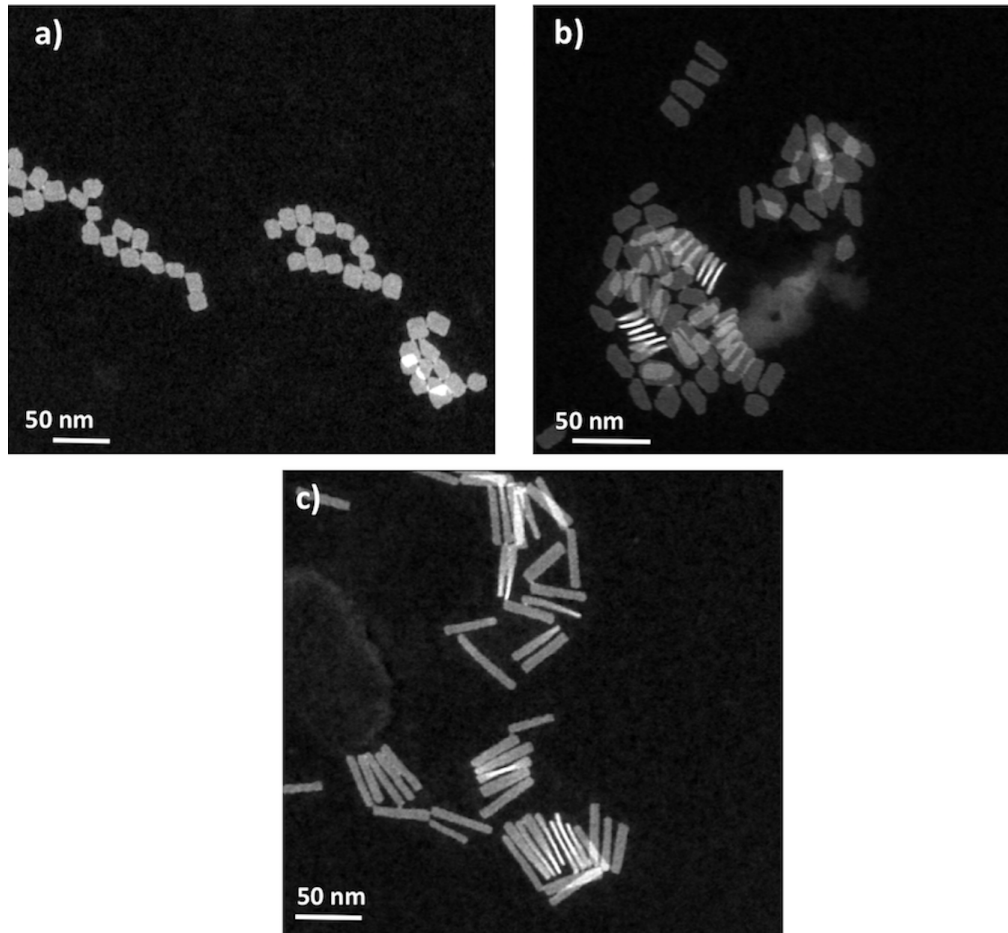
Figure 4.3: HAADF-TEM Images of CdSe core-only NPLs. From (a) to (c) aspect ratio increases.

4.3.2 Optical Characterization

After we characterized the structural features of NPLs, we measured their absorption and PL spectra. In Figure 4.4, from the absorption spectrum, heavy-hole peak positions are demonstrated for three different shapes of 4 ML thick CdSe NPLs. The square NPLs have a heavy-hole peak centered at 513 nm whereas the rectangular NPLs have a heavy-hole peak at 511 nm. Moreover, this peak is shifted to 508 nm for the rod-like NPL.

Furthermore, we observed the same trend for the PL spectra of these NPLs.
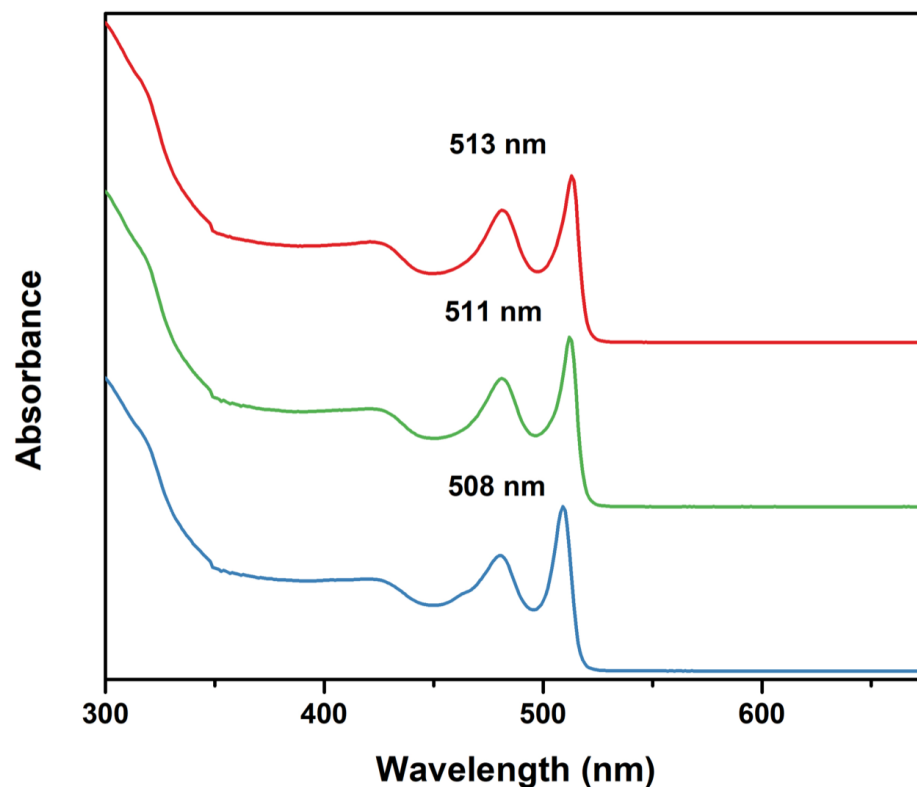
Figure 4.4: Absorption spectra of the size-tuned core NPLs.

As demonstrated in Figure 4.5, the square NPLs have an emission peak at 514 nm, which is common for 4 ML thick CdSe NPLs. Increase in the aspect ratio results in slightly blue-shifted emission profiles.

Until now, it has been shown that excitons in NPLs can freely move in the lateral direction and the strong confinement results from the thickness direction. This situation holds true that when the lengths and widths of the NPLs are larger than exciton Bohr radius of the material. However, if the size of one side can be synthesized comparable to or smaller than the exciton Bohr radius, exciton in these NPLs start 'feeling' the lateral confinement. As the confinement energy increases, band gap energy of the material increases resulting in blue-shifted emission and absorption features.
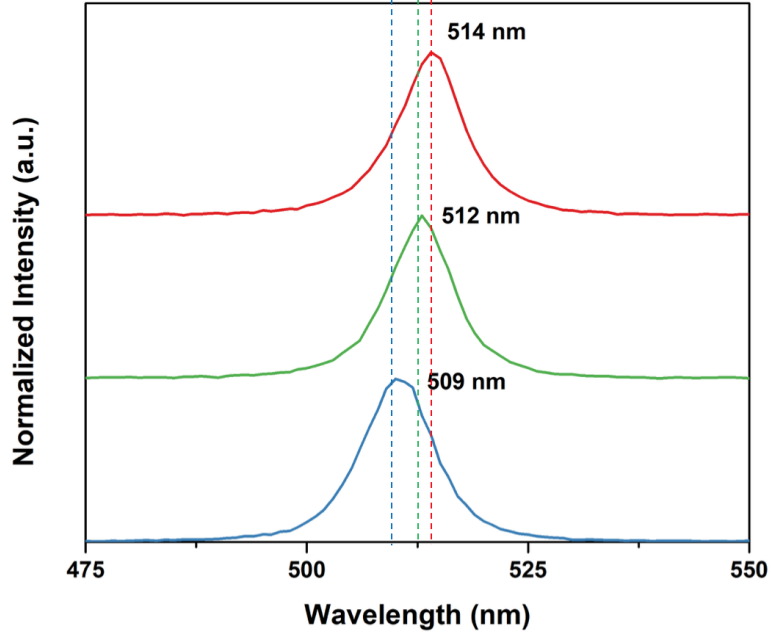
Figure 4.5: PL spectra of the size-tuned core NPLs.

After collecting the absorption and emission spectra, we measured photoluminescence quantum yield (PL-QY) of the samples in solution. PL-QY is measured according to the described method in Section 3.1.4. As seen in Figure 4.6, PL-QY of the samples increases with the increasing aspect ratio.

In addition to these measurements, we characterized PL-lifetime of our core NPLs using the time-resolved fluorescence spectroscopy (TRF) (Table 4.1). TRF measurements were taken in a cuvette filled with the diluted solutions of NPLs. In the literature, core-only NPLs have lifetimes typically between 1.0 and 2.5 ns. In our size-tuned cores, the square NPLs exibit average lifetimes $\tau_{ave} \sim 1.17$ ns, the rectangular NPLs have $\tau_{ave} \sim 2.0$ ns and the rod-like NPLs have $\tau_{ave} \sim 2.49$ ns. We observed an increase in the average lifetimes of the samples with the increasing aspect ratio.

Both PL-QY and the lifetimes are connected to each other with Eq. 4.1 and 4.2:
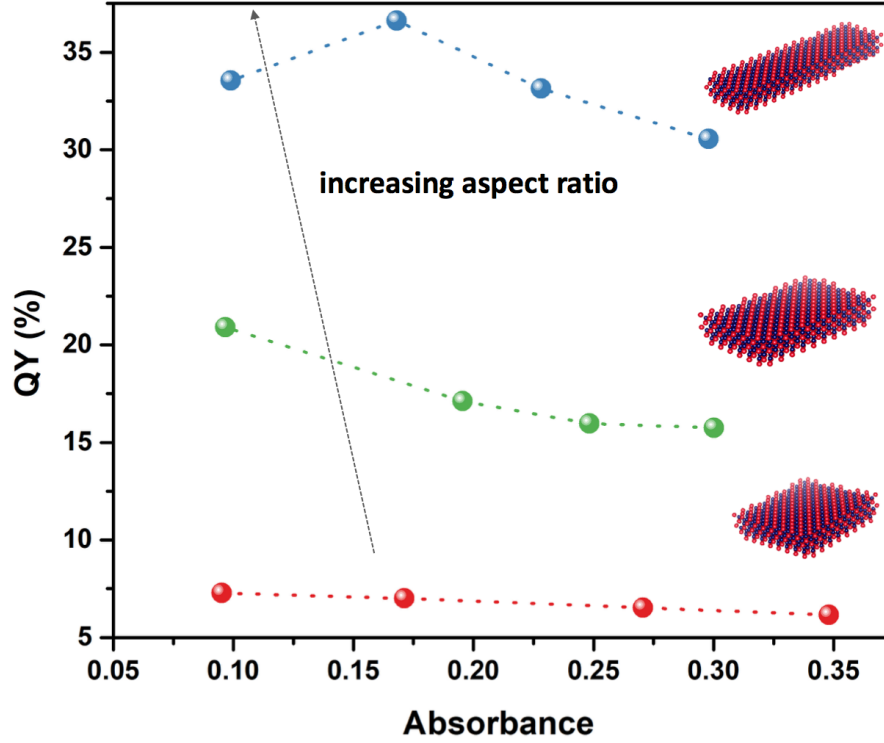
Figure 4.6: PL-QY measurement of the size-tuned core NPLs.

$$\frac{1}{\tau_{avg}} = \frac{1}{\tau_{rad}} + \frac{1}{\tau_{nonrad}} \tag{4.1}$$

$$\%QY = \frac{\frac{1}{\tau_{rad}}}{\frac{1}{\tau_{rad}} + \frac{1}{\tau_{nonrad}}} \tag{4.2}$$

In these equations, τ_{rad} and τ_{nonrad} are the radiative and nonradiative lifetime components. From the square NPLs to the rod-like NPLs, the shape of the structure becomes sharper resulting in better passivation of side walls so that increase both in PL-QY and average lifetimes of the materials could be attributed to their well-passivated shapes.

	A1	τ_1 (ns)	A2	τ_2 (ns)	A3	τ_3 (ns)	A4	τ_4 (ns)	τ_{ave} (ns)
square	232.0	44.0	1156	9.3	19650	0.14	2700	1.53	1.18
rectangular	263.3	42.6	2027	8.6	13160	0.19	3816	2.01	2.01
rod-like	208.3	38.8	2435	7.5	5025	2.40	8656	0.25	2.48

Table 4.1: Analysis of the time-resolved fluorescence decay curves of CdSe NPLs with different aspect ratios.

4.4 Applications

Amplified spontaneous emission (ASE) is observed in luminescent semiconductor nanocrystals, when pumped hard with a pulsed laser if the nanocrystals can be forced into gain. There is no cavity for ASE in the system. However, it gives an indication of possible lasing of the sample if placed in a proper cavity [41], [51].
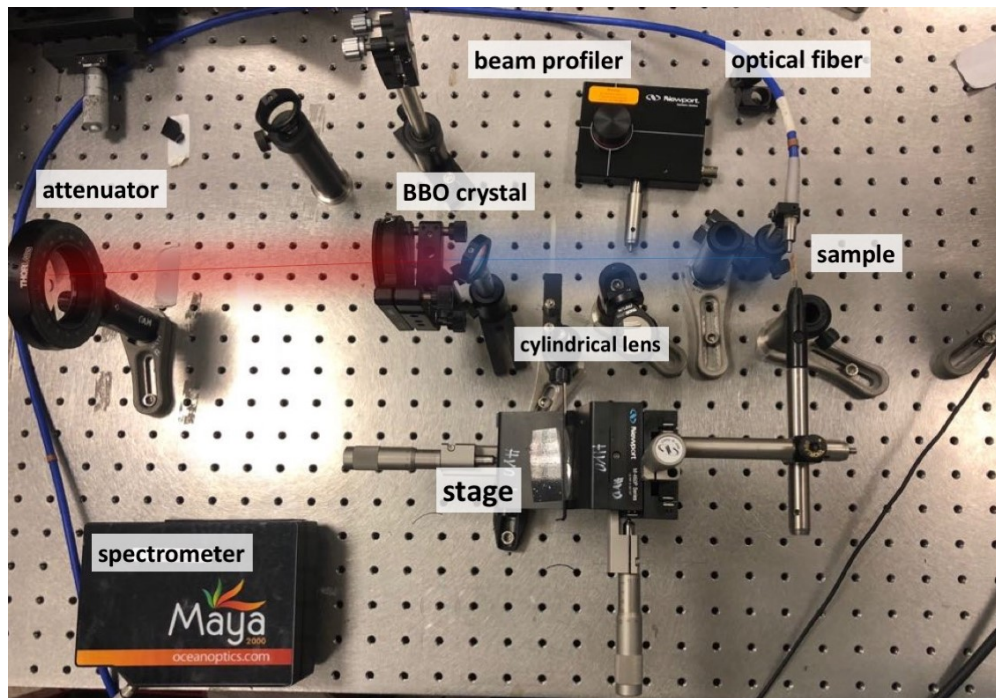
Figure 4.7: Experimental setup for our optical gain studies.

Colloidal NPLs are excellent candidates as a gain medium to build lasers thanks to their remarkable optical properties including narrow spontaneous emission spectrum, suppressed inhomogeneous broadening and giant oscillator strength

[47]. In the literature, different NPL systems having either Type-I or Type-II band alignments were investigated as gain media [51], [52], [53]. In addition to this, the core-only NPLs under consideration were studied as a function of their lateral sizes [48], [49]. However, as mentioned earlier, the consideration of the size effect lacked any additional lateral confinement in these previous works unlike this thesis work, which includes the confinement effect.

Figure 4.8: (a) Photoluminescence spectra of the square CdSe NPLs parameterized with respect to the increasing pump intensity and (b) PL intensity versus pump intensity of the sample.

In this work, after successfully characterizing our NPLs, we investigated their ASE behaviors. Highly dense samples were prepared by spin-coating on clean quartz substrates. Then, samples were excited by using a femtosecond laser beam having a wavelength of 400 nm with a 120 fs pulse width at a 1 kHz repetition rate. Thanks to stripe configuration, the spectra can be collected at the edges via a fiber that is coupled to a spectrometer. Our setup for the optical gain studies is given in Figure 4.7.

In Figure 4.8(a), PL spectra with respect to the pump intensity is given. At lower pulse fluence, only spontaneous emission peak is present, whereas at higher pulse fluence, a narrow ASE peak emerges. We obtained red-shifted ASE peaks with respect to the spontaneous emission, which is common for the NPLs of type-I as in the core-only structure where both electron and hole wave functions are

38
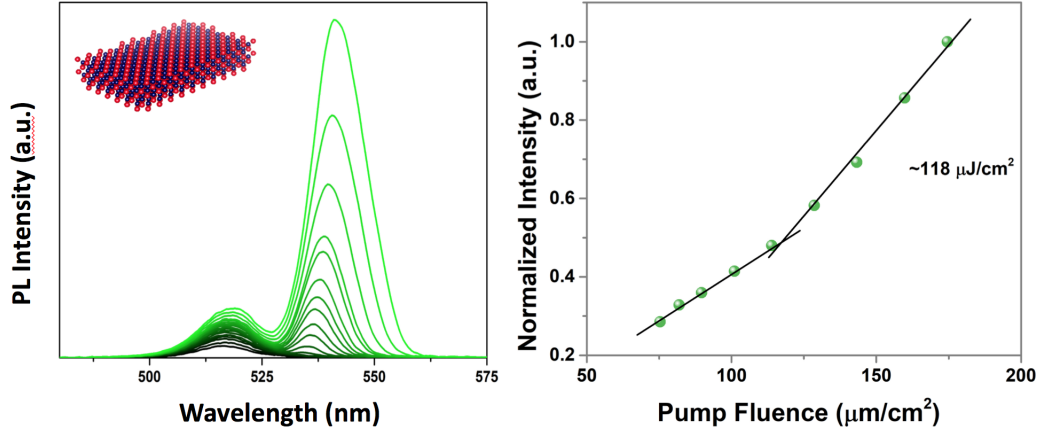
Figure 4.9: (a) Photoluminescence spectra of rectangular CdSe NPLs with respect to increasing pump intensity (b) PL intensity versus pump intensity of the sample.

confined in the core. Moreover, the integrated intensity of each spectrum given in Figure 4.8(a) is constructed as a function of the pump intensity in Figure 4.8(b) and here we can see a clear transition from the spontaneous emission to the stimulated emission (Figure 4.8(b)).

According to Figure 4.8(b), when the pump intensity reached the ASE threshold value of 194 $\mu J/cm^2$, the optical gain was observed. For the rectangular and rod-like samples from Figure 4.9(a) and Figure 4.10(a), optical gain thresholds decreased to 120 $\mu J/cm^2$ (Figure 4.9(b)) and 114 $\mu J/cm^2$ (Figure 4.10(b)), respectively.

Furthermore, by examining the PL spectra with respect to the pump intensity graphs (Figures 4.8(a), 4.9(a) and 4.10(a)), the energy splitting between spontaneous emission and ASE become more explicit with the increasing aspect ratio. The difference between the peak energies of ASE (E_{xx}) and spontaneous emission peaks (E_x) gives us the biexciton binding energy: Δ_{xx}=E_{xx}-2E_x. It can be found that Δ_{xx} equals to -2.46 eV for the square NPLs, -2.50 eV for the rectangular NPLs and -2.52 eV for the rod-like NPLs. Biexciton binding energy thus increases with the aspect ratio. This may indicate that reason could be that biexcitons become more attractive as opposed to being repulsive as a result of the additional confinement.
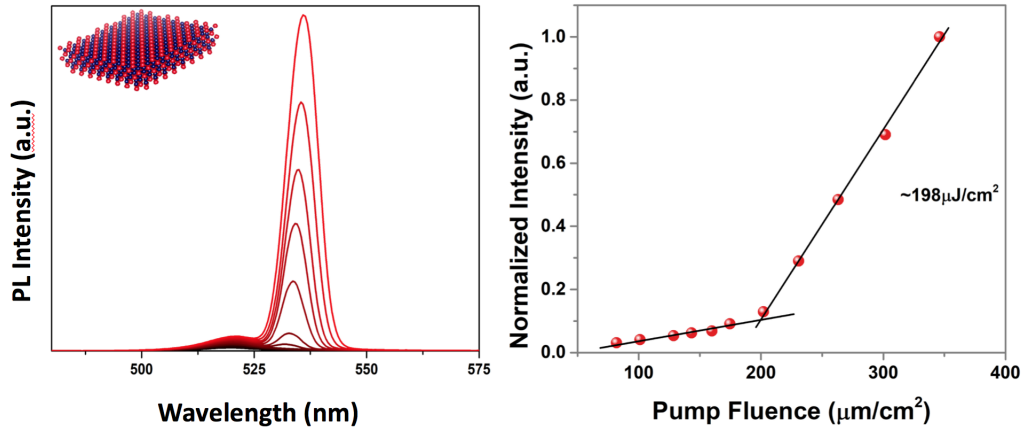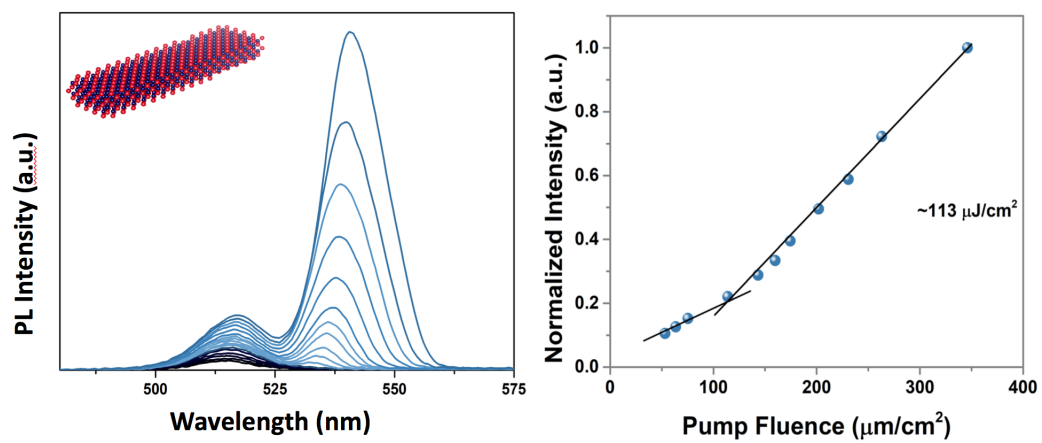
Figure 4.10: (a) Photoluminescence spectra of the rod-like CdSe NPLs parameterized with respect to the increasing pump intensity and (b) PL intensity versus pump intensity of the sample.

Chapter 5

Synthesis and Characterization of Colloidal Multiple and Alloyed-Crown Quantum Wells

5.1   Motivation

Unique optical properties of nanoplatelets including giant oscillator strength, narrow emission bandwidth and ultrafast radiative lifetime can be attributed to their precise vertical thickness. Also NPLs possess large linear and nonlinear absorption cross-sections which is related to their growt1h in the lateral directions. Furthermore, optical features of NPLs can be varied by different heterostructures including core/shell [38] and core/crown [36]. In the case of core/shell NPLs, the shell is grown on top of the core by increasing its thickness. In the core/crown NPLs, the lateral growth occurs around the periphery, without altering its thickness. By growing these heterostructures, the relative positions of conduction and valence band offsets can be changed and different electronic band alignments of either type-I, quasi type-II or type-II can be obtained.

In the type-I electronic structures, both electron and hole wave functions are

confined in the same part of the structure resulting in large oscillator strengths and shorter radiative lifetimes compared to type-II NPLs. In the quasi type-II NPLs, one of the carrier wavefunction is delocalized over the entire structure whereas the other confined in the only one part. In CdSe/CdS core/crown NPLs, electron is delocalized over the entire structure due to the close proximity of the conduction band offsets of CdSe and CdS and hole is confined in the core. In the type-II NPLs, spatially indirect exciton recombines at the charge transfer state. Since the electron and hole wave functions are localized in different parts of the structure, their radiative recombination lifetime is much longer than typical type-I NPLs. For instance, the exciton lifetime reaches up to 190 ns in CdSe/CdTe core/crown NPLs [54]. Another type-II example is $CdSe/CdSe_{1-x}Te_x$ core/alloyed-crown structures, which has received great attention. Their type-II band alignment accompanied by improved features compared to pure CdSe/CdTe NPLs have brought about their characteristic optical behaviors including bicolor emission, high quantum efficiency and unique multiexciton behavior [16],[55], [56].

Figure 5.1: Our precipitated $CdSe/CdSe_{1-x}Te_x$ core/alloyed-crown NPLs in solution. They form gel-like structures.

However, these core/alloyed-crown type-II materials are unstable in solution, forming gels (Figure 5.1). Eventhough their surface is coated with organic capping ligand (oleic acid) they show weak solubility in nonpolar solvents. After they are synthesized, they tend toform stacks easily, which makes them difficult to use in possible applications despite their remarkable properties. We hypothesized that there could be two reasons behind their unstability, which are either

their electronic structure or their extremely uniform, well-defined shapes. Since these NPLs have type-II band alignment, carriers localize in different parts of the structure. As a result, localized charge distribution may result in forces stronger than Van der Waals. Another root cause could be their perfect symmetrical shape. According to Abecassis et al., only the NPLs having well-defined edges self-assemble into superparticles or stack structures. [57] Since our NPLs have razor-sharp periphery, their unstability could result from their well-defined shape.

Here, to avoid their unstability, we propose and demonstrate to grow a second crown made of CdS around the periphery of CdSe/CdSe$_{1-x}$Te$_x$ ($x \leq 50$) core/alloyed-crown structures. By coating CdS, we find that we achieve high stability in solution. Since CdS band offset is located at higher energies compared to the band offsets of CdSe$_{1-x}$Te$_x$, we preserve their emission features and we further increase their absorption cross section. Following the synthesis, here we characterized their optical and structural properties. Moreover, as a possible application, we studied their exceptional optical gain performances.
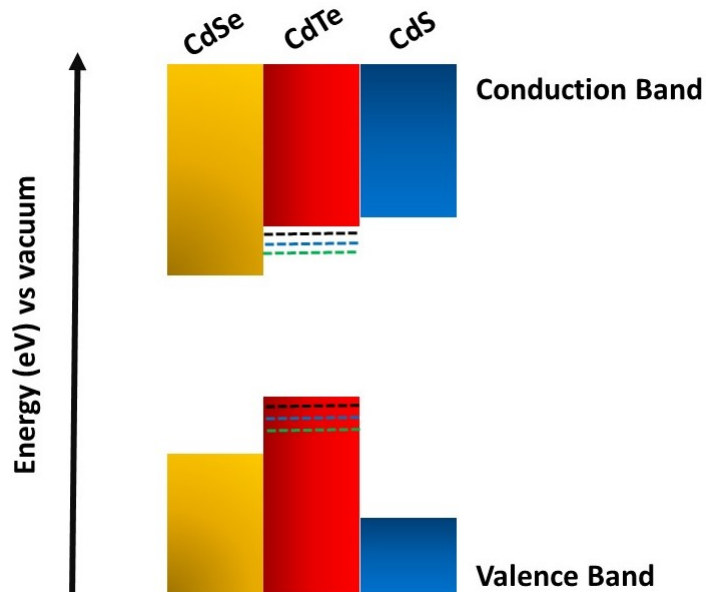

Figure 5.2: Bulk energy band gaps of CdSe, CdTe and CdS semiconductors.

5.2 Experimental

5.2.1 Chemicals

Chemicals and solvents that were used in the synthesis are cadmium acetate dihydrate $[Cd(Ac)_2.2H_2O]$ ($\geq 98\%$), technical-grade 1-octadecene (ODE), elemental tellurium (Te), selenium (Se), sulfur (S) (99.998% all are trace metals basis), technical-grade oleic acid (OA) (90%), trioctyl phosphine (TOP) (technical grade $\geq 90\%$). Toluene, ethanol, and hexane were purchased from Sigma Aldrich.

5.2.2 Colloidal Synthesis of Core-Only Quantum Wells

Cadmium precursor for the core synthesis is cadmium myristate and its synthesis was explained in detail in Section 4.2.2. To synthesize 4 ML thick CdSe NPLs, 170 mg of cadmium myristate, 12 mg Se and 15 mL of ODE were loaded in a flask. The mixture was degassed and mixed with the help of magnetic stirrer under vacuum at $90°C$ around 1 hour. After degassing, the temperature of the solution was increased to $237°C$ under inert atmosphere. At $195°C$, 45 mg of $[Cd(Ac)_2 2H_2O]$ was added. After 10 min growth at $240°C$, 1 mL of OA was injected to stop the reaction and the solution was cooled to room temperature by water quenching. At room temperature, 5 mL of hexane was injected for the better dissolution of NPLs. Then NPLs were cleaned and stored in hexane.

5.2.3 Preparation of Isotropic Growth Solutions

Selenium and tellurium precursors were prepared as 1 M inside the glovebox (under oxygen-free atmosphere). 1 mmol elemental Se was dissolved in 1 mL TOP and mixed with a magnetic stirrer for 20 minutes to obtain 1 ML solution. For the Te precursor, 1 mL TOP was added to 1 mmol Te and then the solution was stirred at $85°C$ for around 4-5 hours.

5.2.4 Preparation of Anisotropic Growth Solutions

For the lateral growth of CdS crown region, Cd and S precursors were prepared according to the well-known procedure with slight modifications [16]. 480 mg of $[Cd(Ac)_2 . 2H_2O]$, 340 μL of OA and 2 mL of ODE were stirred at $120°C$ under ambient atmosphere and regularly sonicated until a whitish homogeneous gel is formed. As the sulfur source, 0.15 M S in ODE was prepared at $120°C$ under ambient conditions.

5.2.5 Colloidal Synthesis of Core/Alloyed-Crown Type-II Quantum Wells

The core/alloyed-crown NPLs were synthesized according to a well-known procedures with slight modifications [58], [56]. A 25 mL flask was used to synthesize $CdSe/CdSe_{1-x}Te_x$ core/alloyed-crown NPLs. 1.5 mL of CdSe NPLs solution having optical density ~ 0.9 at the 1st excitonic peak, was cleaned once with ethanol and dissolved in 3.5 mL ODE. Then, the core dissolved in an ODE, 400 μL $[Cd(Ac)_2 . 2H_2O]$ and 45 μL of oleic acid were placed in the flask and slowly degassed at RT around 40 min. Under argon flow, the temperature of the solution was raised to $215°C$ and the mixture of TOP-Se, TOP-Te, and ODE (0.025 M) was injected at a rate of 2 mL/h. When the injection was completed, the solution was kept at this temperature for 1 more minute and 0.5 mL oleic acid was added. Then, the reaction was swiftly cooled down to RT, 5 mL hexane was added for better dissolution and kept as-synthesized without further cleaning.

5.2.6 Colloidal Synthesis of Core/Alloyed-Crown/Crown Quantum Wells

To grow the CdS around the periphery of Type-II NPLs, an anisotropic growth mixture was prepared as described in Section 5.2.4. 8 mL of the as-synthesized

Type-II NPL solution is cleaned with EtOH and dissolved in 0.4 mL hexane and 4 mL ODE. The solution was placed in a 25 mL flask with 50μL of OA and degassed at RT. Under Ar flow, the temperature was set to $225°C$ and at $180°C$ the injection process of the Cd-S precursor mixture was started. When 0.35 mL of precursor was injected, the reaction was cooled to RT and 5 mL hexane was added. The solution was centrifuged at 3,000 rpm for 3 min. Normally after CdS coating, during the centrifuge, there occurs almost no precipitation. Finally, the supernatant was washed with ethanol at 6,000 rpm for $\sim$ 6 min, and the precipitate was dissolved in toluene.

5.3   Results and Discussion

5.3.1   Optical Characterization

First, we synthesized 4 ML thick CdSe core NPLs. In Figure 5.3, from the absorption and PL spectra, we can see that there is no formation of other families of NPLs. Our NPLs are purely 4 ML thick and their PL peak is centered at $\sim$513 nm having an FWHM of 10 nm.

After synthesizing the core NPLs, we prepared type-II NPLs as described in Section 5.2.5. Pure 4 ML thick CdTe has an absorption peak centered at $\sim$ 553 nm. Therefore, the absorption peak at lower energies corresponds to an alloyed type-II crown. Depending on the amount of Te introduced into the crown, the absorption peak of the crown changes as a result of 'the band mixing effect.

As an example, absorption and PL spectra of $CdSe/CdSe_{0.6}Te_{0.4}$ are presented in Figure 5.4. In addition to the CdSe core peaks, the alloyed-crown peak can be seen at 582 nm. Since these NPLs have type-II band alignment and the emission comes from the charge transfer state [50]. PL spectrum shifts from 513 nm to 591 nm and inhomogeneous broadening occurs.
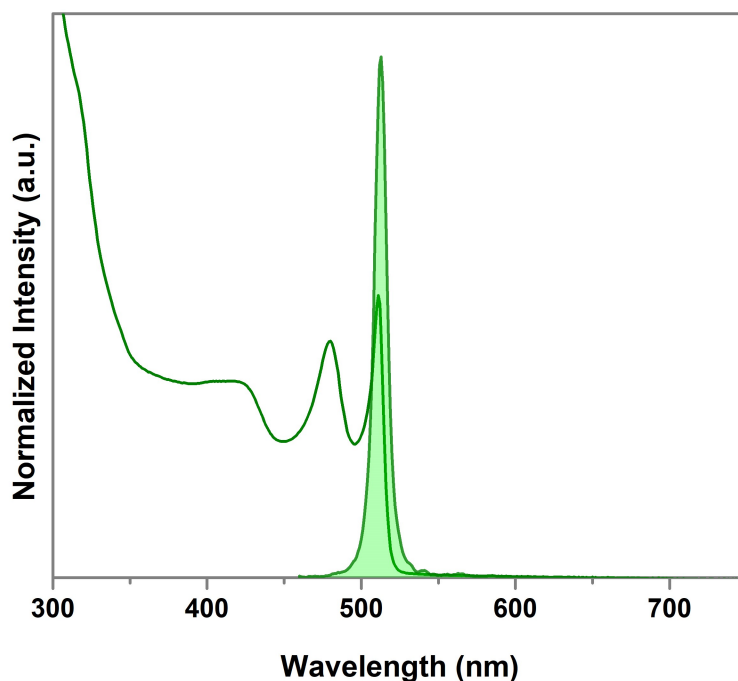
Figure 5.3: Absorption and photoluminescence spectra of 4 ML thick CdSe NPLs, which are used for type-II synthesis.

To prove the uniform alloyed-crown formation around the periphery of CdSe core NPLs, we performed photoluminescence excitation spectroscopy (PLE). PLE is an important characterization tool to determine the quality of the synthesis and it should exactly resemble the absorption spectrum if the crown growth is successful. In Figure 5.5, PLE spectrum taken at the PL peak position of the $CdSe/CdSe_{0.6}$ $Te_{0.4}$ is shown. The PL spectrum is found very similar to the absorption spectrum, which indicates the successful crown formation.

These NPLs are unstable in solution and our purpose is to stabilize them by CdS crown. 4 ML thick CdS NPLs have an absorption peak centered at ~ 405 nm. In Figure 5.6, the peak located at higher energies corresponds to CdS. Moreover, there is only 3-4 nm shift in the PL, which is attributed to the change in the dielectric constant of effective medium. Moreover, to check whether any separate CdS nucleation occurred, the PLE spectroscopy was used (Figure 5.6). Measurements were taken at three different emission wavelengths and all three spectra resemble the absorption spectrum of the same NPLs.
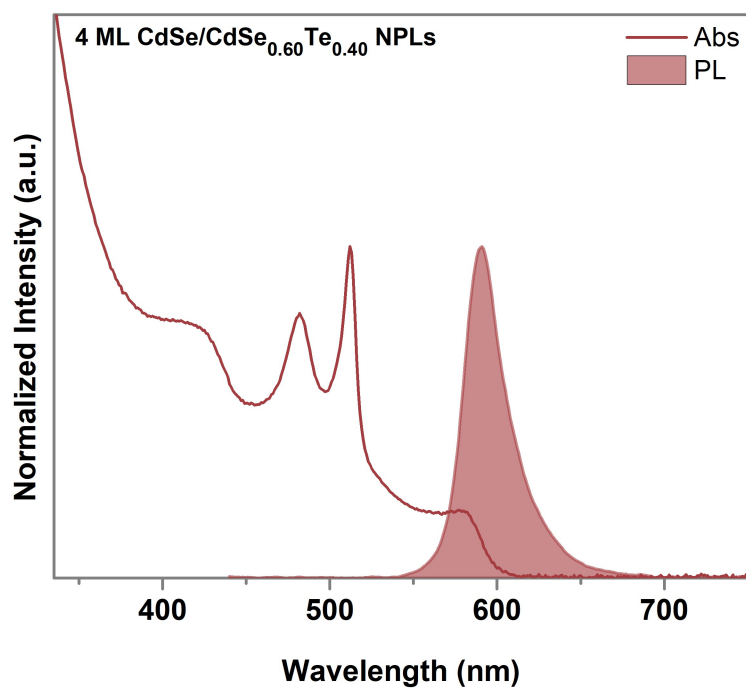
Figure 5.4: Absorption and PL spectra of CdSe/CdSe$_{0.6}$Te$_{0.4}$ core/alloyed-crown NPLs.
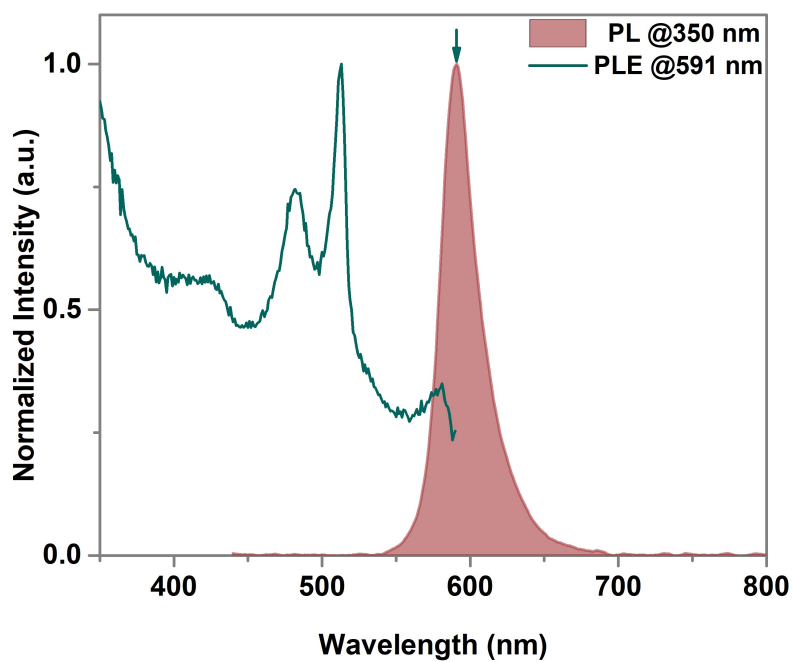

Figure 5.5: PL and PLE spectra of CdSe/CdSe$_{0.6}$Te$_{0.4}$ core/alloyed-crown NPLs.
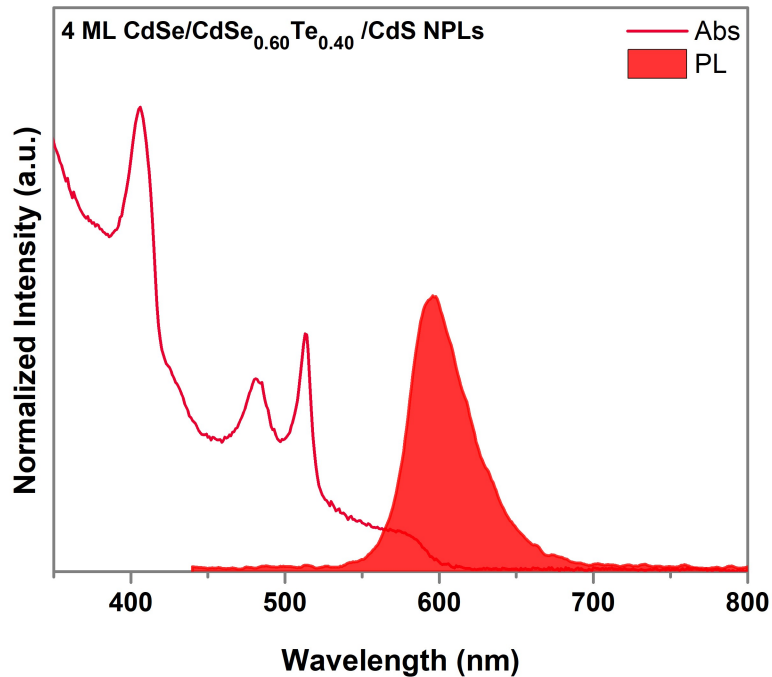
Figure 5.6: Absorption and PL spectra of $CdSe/CdSe_{0.6}Te_{0.4}/CdS$ core/alloyed-crown/crown NPLs.

In addition to $CdSe/CdSe_{0.6}Te_{0.4}/CdS$ core/alloyed-crown/crown NPLs measurements, we coated CdS crown around the periphery of $CdSe/CdSe_{1-x}Te_x$ NPLs having compositions of x=0.05, x=0.10, x=0.25 and x=0.50. In Figure 5.8, absorption and PL spectra of these core/alloyed-crown and core/alloyed-crown /crown are presented. Among the samples, in $CdSe/CdSe_{0.5}Te_{0.5}/CdS$ NPLs, seperate CdS nucleation occured, as can be seen at the tail of the PL spectrum at higher photon energies. We further confirmed the CdS formation by the PLE spectroscopy that can be seen in Figure 5.9(d).

Moreover, to demonstrate the unstability nature of the core/alloyed-crown NPLs, a stability test was performed. The sample having an optical density of around one was taken in a cuvette and PL intensities of the samples were recorded as a function of the time inside the integrating sphere.We conducted these experiments for 24 hours using three different sets of the core/alloyed-crown samples. The CdS-coated multi-crown structures showed higher stablities than the bare type-II NPLs (Figures 5.10(a), (b) and (c)).
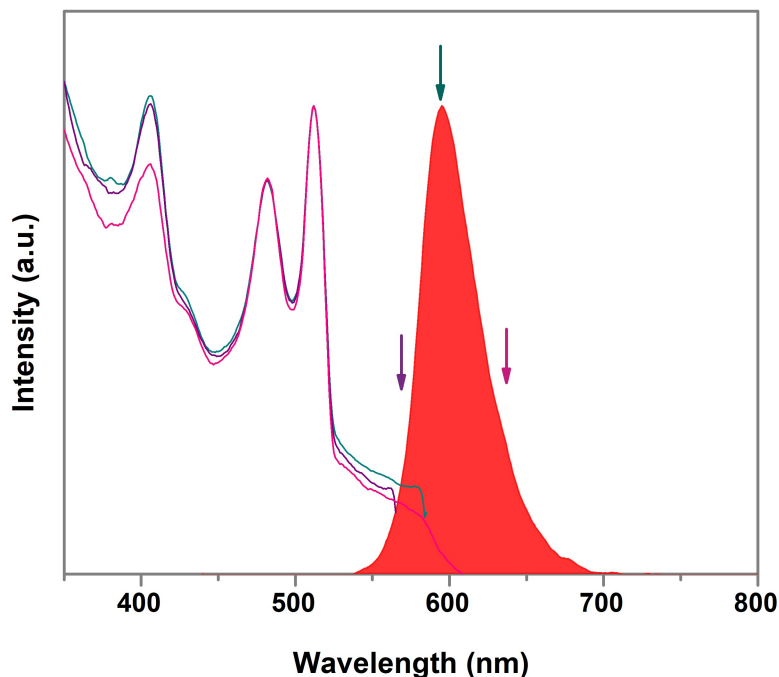
Figure 5.7: PL and PLE spectra of $CdSe/CdSe_{0.6}$ $Te_{0.4}/CdS$ core/alloyed-crown/crown NPLs. PLE measurements were taken at three different PL positions.

5.3.2 Structural Characterization

Transmission electron microscopy (TEM) plays a significant part in the characterization of NPLs. By using TEM, the size, shape, and thickness of the NPLs can be determined. In this work, after synthesizing CdSe 4 ML core-only NPLs, we imaged them under an electron microscope in HAADF mode. Our NPLs have a long side of $\sim 18.7 \pm 1.8$ nm and a short side of $\sim 10.2 \pm 1.5$ nm (Figure 5.11). Their shapes were initially nonuniform; however, the core shape does not have any effect on the shape of type-II NPLs, which all have well-defined shapes.

After characterizing core NPLs, we used them as a seed to grow $CdSe_{0.95}$ $Te_{0.05}$ crown around them. The type-II synthesis was carried out according to the procedure described in Section 5.2.5. From the TEM images of the synthesized type-II NPLs, their razor-sharp corners can be seen (Figure 5.12).

Figure 5.8: Absorption and PL spectra of CdSe/CdSe$_{1-x}$Te$_x$ core/alloyed-crown NPLs and those with their CdS crowns at a) x=0.05, b)x=0.10, c)x=0.25, and d)x=0.50.

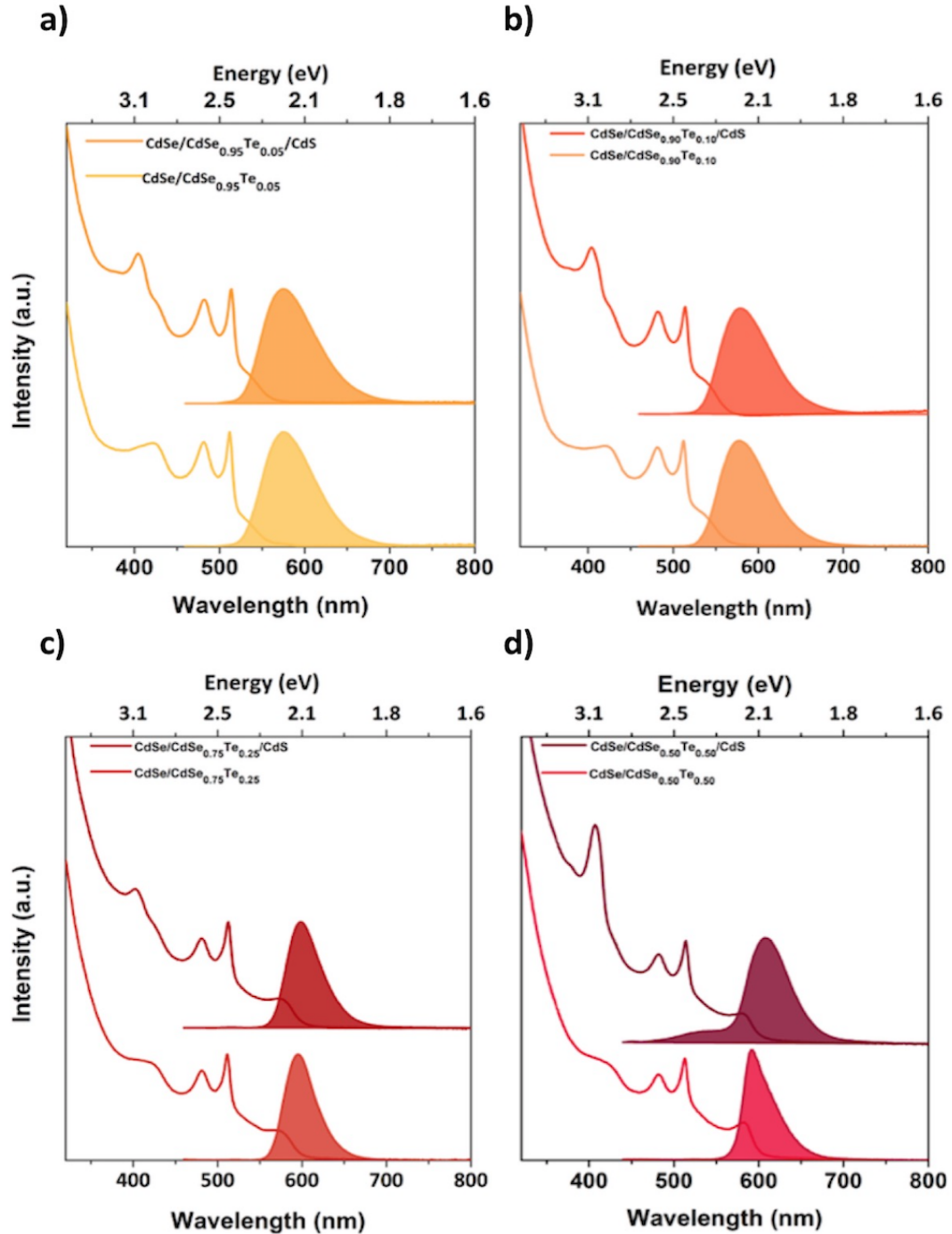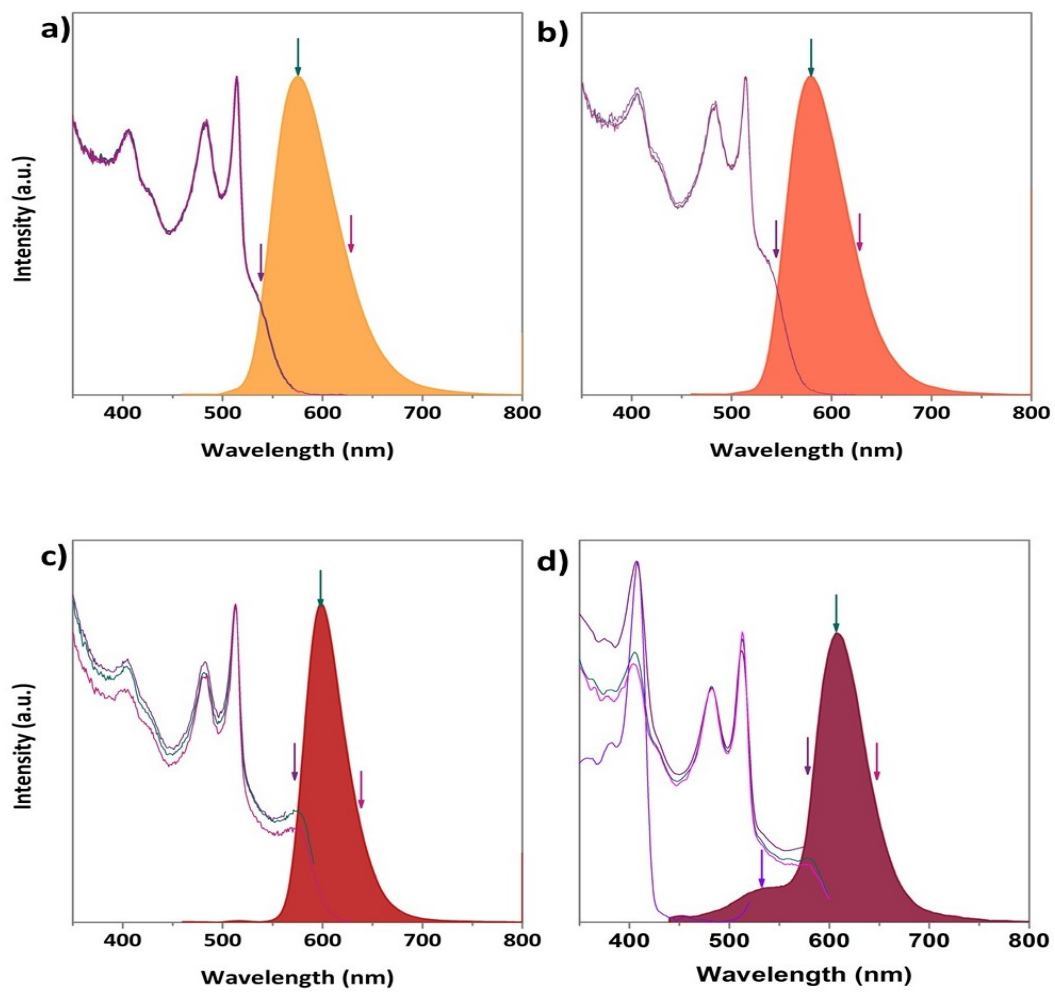Figure 5.9: PL and PLE spectra of CdSe/CdSe$_{1-x}$Te$_x$/CdS core/alloyed-crown/ crown NPLs at a) x=0.05, b)x=0.10, c)x=0.25, and d)x=0.50.
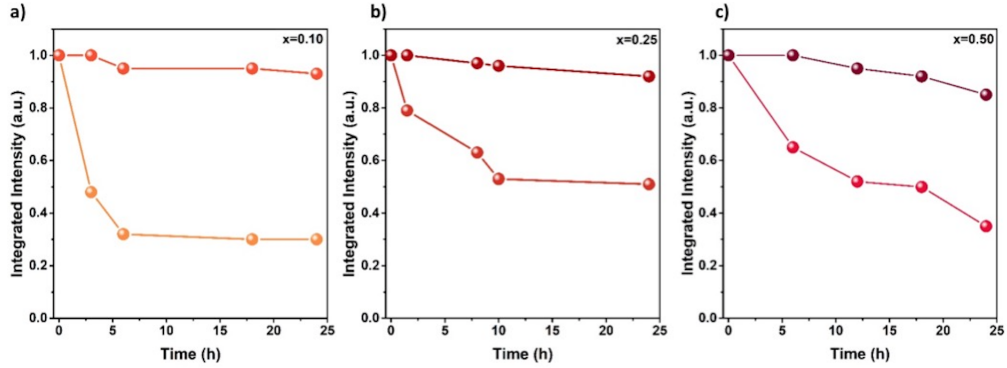
Figure 5.10: Integrated intensity versus time for $CdSe/CdSe_{1-x}Te_x$ core/alloyed-crown NPLs and those with their CdS crowns. In all graphs, a sudden decrease is seen for the core/alloyed-crowns, whereas intensity of the CdS-coated NPLs is reasonably stable over time.

As mentioned previously, these NPLs are not stable in solution and to enhance their stability, we grew CdS around their periphery. In Figure 5.13, the CdS-coated core/alloyed-crown/crown NPLs can be seen. Compared to $CdSe_{0.95}$ $Te_{0.05}$ crown, the growth of CdS crown is not uniform. We hypothesize that the reason for the nonuniform formation of CdS crowns is the activity of its precursor. However, it can be seen that their perfect symmetrical shape is disrupted, which may help to avoid forming stacks of NPLs. From the corners, the size of the CdS crowns is around 3-4 nm. Similarly, the CdS crown growth was applied to other compositions of the alloyed type-II crowns (for x=0.10, 0.25, 0.4, and 0.5), and their HAADF-TEM images can be found in Figure 5.15. It can be seen that their size distribution is quite uniform and monodisperse.
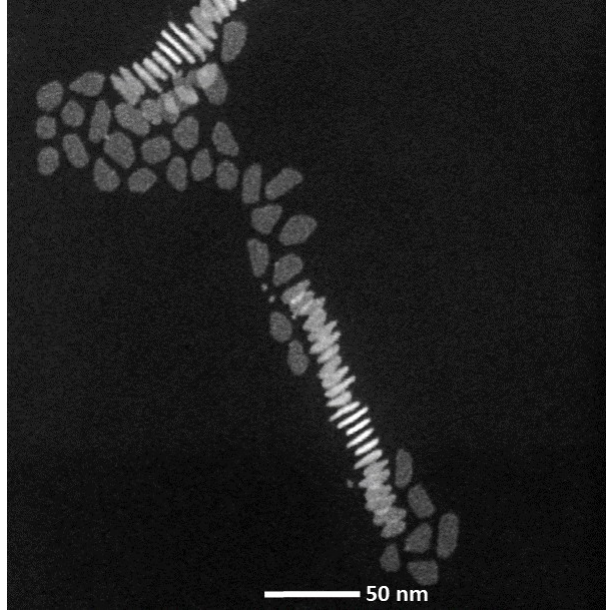
Figure 5.11: HAADF-TEM image of 4 ML thick CdSe NPLs.

For the analysis of the elemental composition of the CdS crown, we performed energy dispersive X-ray spectroscopy (EDX) under TEM (Figure 5.5). We collected the spectrum exactly at the presumed CdS region, and only Cd and S elements can be seen. According to the analysis, we found 53% S and 47% Cd, which is almost 1:1 ratio as expected.

Furthermore, we also analyzed the composition of the crown region with X-ray photoelectron spectroscopy (XPS). In the literature, there is a good correlation between the injection amount of Se and Te and the composition of the crown [56],[58]. However, to be precise, we measured our core/alloyed-crown samples under XPS. After measuring the core-only and core/alloyed-crown NPLs if the sizes of the core and core/alloyed-crown NPLs are known, their composition can be calculated as follows:

$$Te_{crown} = Te_{measured} \qquad (5.1)$$

$$Se_{crown} = Se_{measured} - Se_{core} \qquad (5.2)$$

$$Se_{core} = Se_{measured} \times \frac{Area_{core}}{Area_{total}} \qquad (5.3)$$
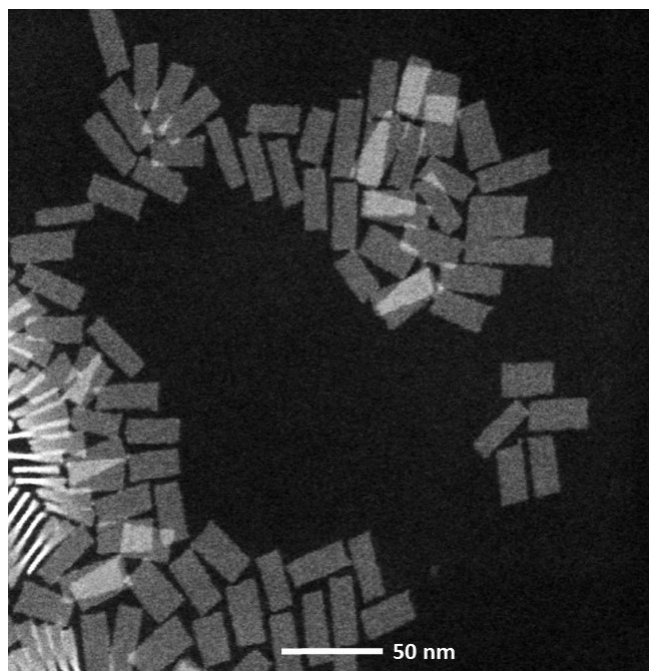
Figure 5.12: HAADF-TEM image of 4 ML CdSe/Cd $Se_{0.95}$ $Te_{0.05}$ core/crown NPLs.
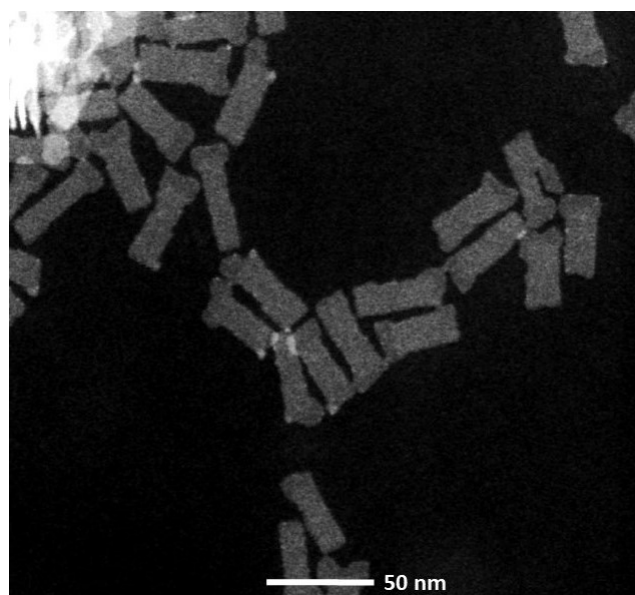
Figure 5.13: HAADF-TEM image of 4 ML CdSe/Cd $Se_{0.95}Te_{0.05}$/CdS core/alloyed-crown/crown NPLs.
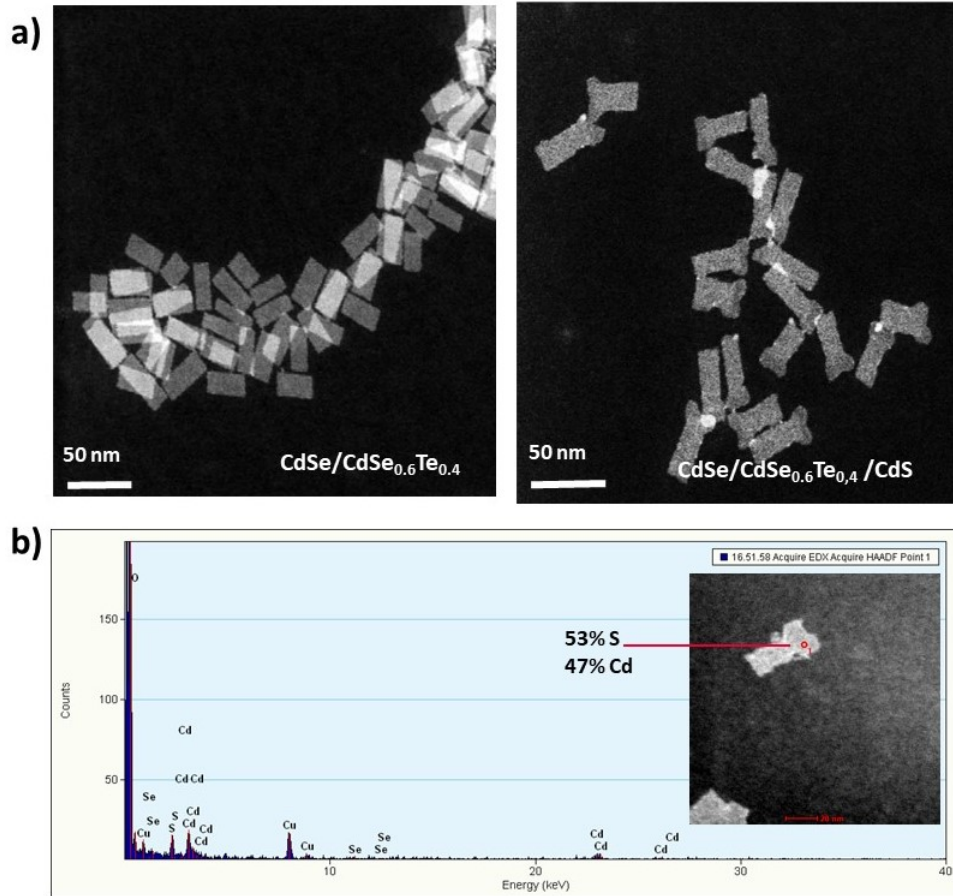
Figure 5.14: (a)HAADF-TEM image of 4 ML CdSe/Cd $Se_{0.6}Te_{0.4}$ core/alloyed-crown and CdS-coated core/alloyed-crown/crown NPLs and (b) EDX analysis performed on CdSe/Cd $Se_{0.6}Te_{0.4}$/CdS core/alloyed-crown/crown NPLs. CdS formation is verified.

$$x = \frac{Te_{crown}}{Te_{crown} + Se_{crown}} \tag{5.4}$$

The measured Te and Se compositions in the equations are the total amounts found by measuring the core/alloyed sample. As an example, XPS spectrum of $CdSe/CdSe_{0.90}Te_{0.10}$ is given in Figure 5.16. Three spectra are collected from the 3d peaks of elements. By removing the backgrounds from each spectrum, atomic percentages of Cd, Se, and Te can be quantified and the composition of the crown can be calculated from the above equations.

Moreover, to confirm the presence of sulfur, we took the XPS spectra of the

56
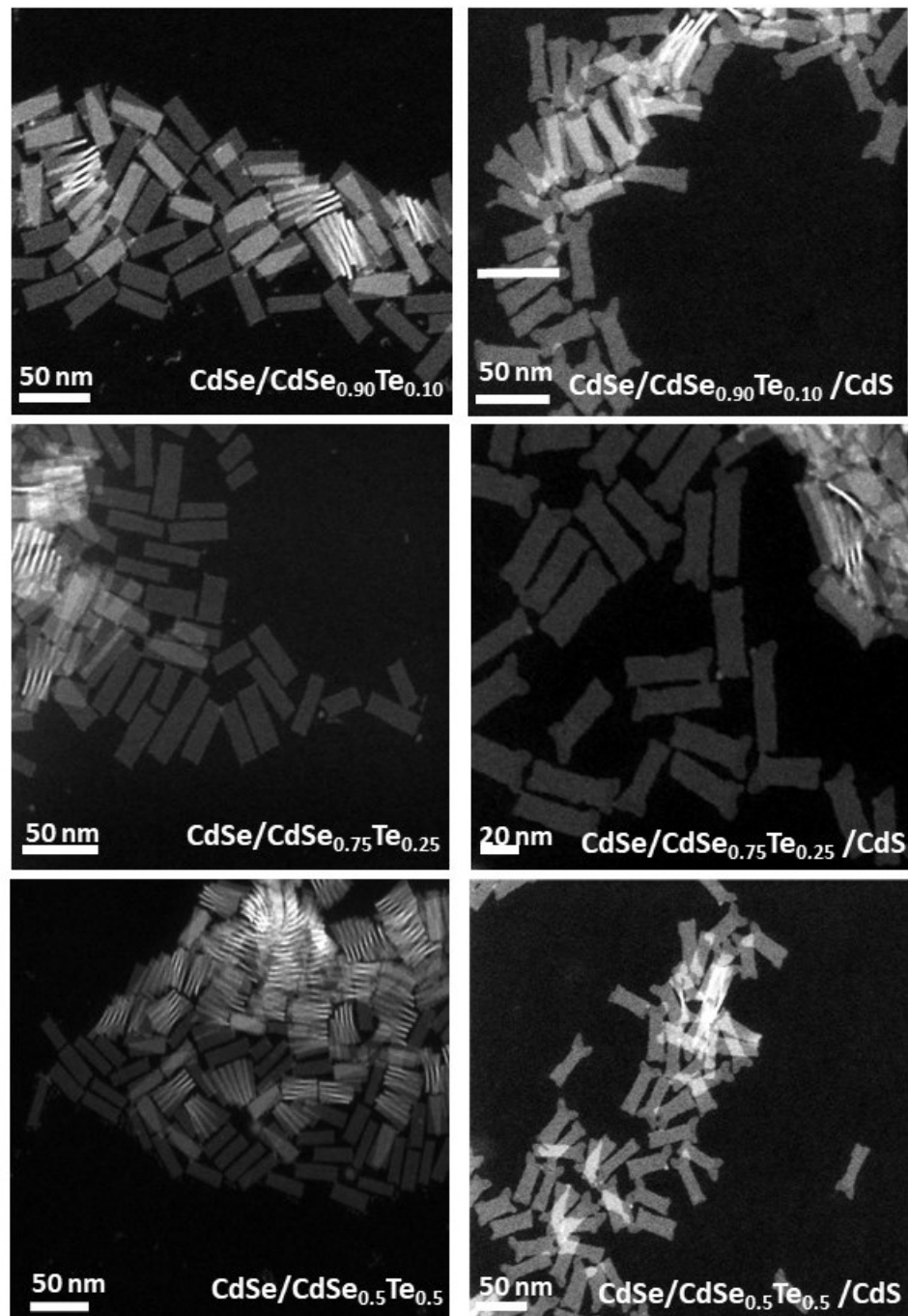
Figure 5.15: HAADF-TEM images of CdSe/Cd$Se_{1-x}Te_x$/CdS NPLs for x=0.10, 0.25, and 0.5.
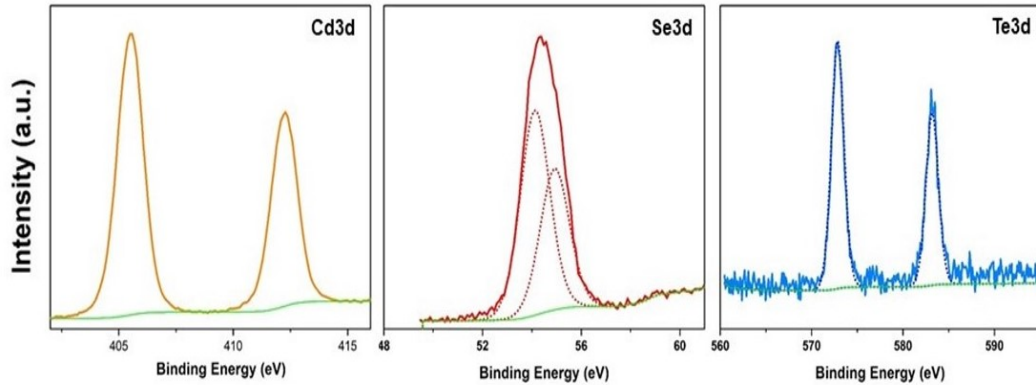
Figure 5.16: XPS spectra of CdSe/Cd$Se_{0.90}Te_{0.10}$ NPLs.

	Long axis	Std. dev.	Short axis	Std. dev.	Lateral area	Cd total	Se total	Te total	Te crown	Se crown	Atomic % of Te (crown)	Atomic % of Se (crown)
core	18.70	1.85	10.28	1.53	192.32	52.38	47.62	-	-	-	-	-
0.05	32.36	3.83	12.62	1.42	408.34	43.03	55.99	0.98	0.98	26.37	0.04	0.96
0.1	42.77	4.64	11.25	1.81	481.18	47.74	49.05	3.22	3.22	19.60	0.14	0.86
0.25	37.21	7.68	10.67	1.87	397.06	48.87	44.36	6.77	6.77	21.49	0.24	0.76
0.4	32.12	5.03	15.02	2.13	482.54	64.10	27.89	8.01	8.01	11.12	0.42	0.58
0.5	51.77	7.40	13.09	2.29	677.52	52.17	36.86	10.97	10.97	10.46	0.51	0.49

Table 5.1: XPS analysis of the chemical compositions of CdSe/CdSe$_{1-x}$Te$_x$ core/crown NPLs having different crown compositions.

core/alloyed-crown/crown samples. However, the binding energies of sulfur coincide with Se peaks. Therefore, we checked the sulfur's SLM1 peak, which corresponds to its Auger peak. However, XPS is not Auger spectroscopy; therefore, it could be misleading to calculate the amount of sulfur present in the structure. In Figure 5.17, sulfur SLM1 peak of the core/alloyed-crown is unavailable and that of the core/alloyed-crown/crown NPL is present. The presence of sulfur in the core/alloyed-crown/crown is thus easily distinguished from the spectrum.
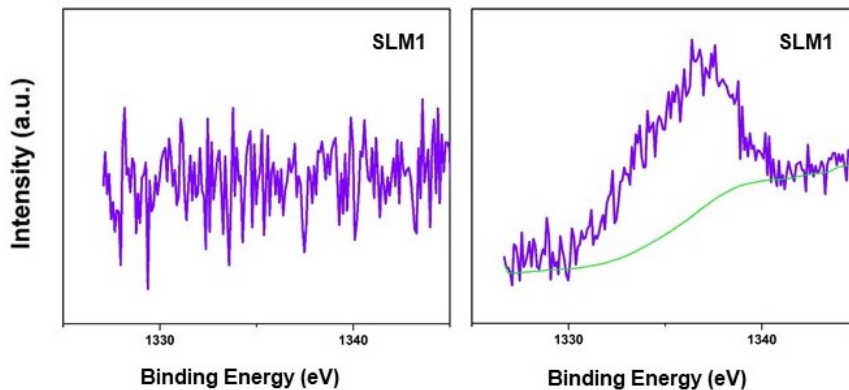
Figure 5.17: XPS spectra of the core/alloyed-crown and the core/alloyed-crown/crown NPL sample for x=0.10.

5.4 Applications

As discussed previously, NPLs are highly promising materials as optical gain media. Compared to the type-I NPLs, the type-II NPLs are more advantageous in different aspects fromthe gain point of view. The type-II NPLs have low Auger rates and long exciton lifetimes resulting from the recombination of spatially indirect excitons. Thanks to these properties, their performance for gain has been found remarkable. Previously, our group reported in [55] that type-II NPLs are highly attractive especially for tunable laser applications owing to their low ASE threshold values as low as 26μJ.

However, their unstability in solution or their tendency to form stacks both in solution and film limits their optical performance levels. It has been shown that the stack form of these NPLs causes additional light scattering in the solid film. This undesired effect increases the waveguide losses, which leads to diminishing modal gain coefficients.

In this thesis, we showed that, by additionally growing CdS crown, these type-II NPLs are stabilized and they are less prone to stacking. After they become stabilized, we examined their optical gain properties. To study ASE of these samples, we prepared solid films of the core/alloyed-crown/crown heterostructures by spin coating. Then, they were optically pumped with a femtosecond laser having
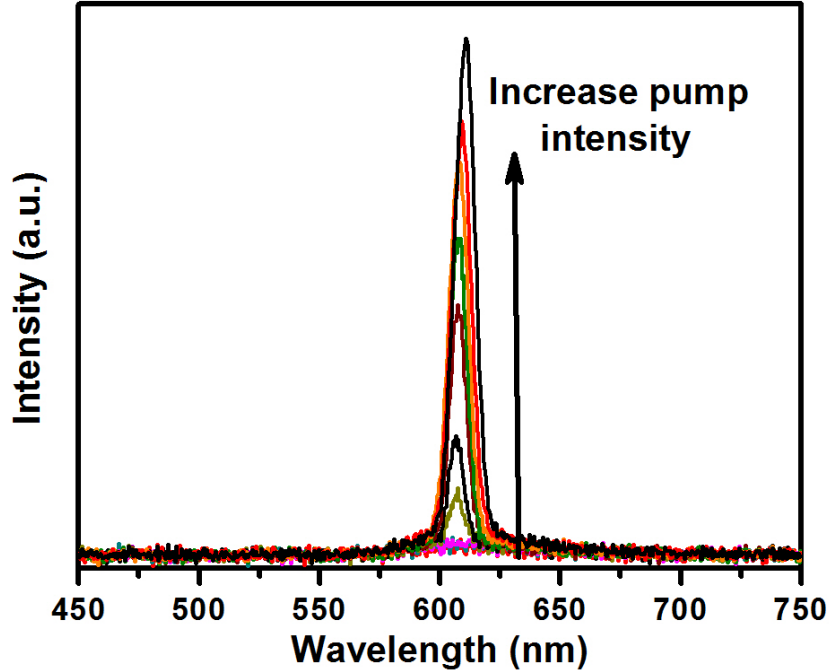
Figure 5.18: Emission spectra of our $CdSe/CdSe_{0.75}Te_{0.25}/CdS$ core/alloyed-crown/crown NPLs parameterized with respect to the increased pump intensity.

a wavelength of 400 nm at a 1 kHz repetition rate and their emission spectra were collected as a function of the pump intensity. Figure 5.18 presents the PL intensity of the $CdSe/Cd Se_{0.25} Te_{0.25}/CdS$ core/alloyed-crown/crown NPLs at the increasing pump intensity levels. As can be seen in Figure 5.18, at lower pump intensities, the spontaneous emission dominates with an FWHM of ~ 55 nm whereas, at higher pump intensities, a ASE peak emerges with an FWHM ~ 11 nm. Here, the position of the ASE peak is slightly blue-shifted compared to the spontaneous emission peak. These blue-shifted ASE peaks demonstrate multiexciton gain, which is typical for type II-like structures.

Figure 5.19 depicts the integrated PL intensities from our $CdSe/CdSe_{0.25}Te_{0.25}/CdS$ core/alloyed-crown/crown sample as a function of the pump intensity with an optical gain threshold of 4.6 $\mu J/cm^2$. To the best of our knowledge, this is one of the lowest threshold values for all semiconductor nanocrystals. Moreover, the
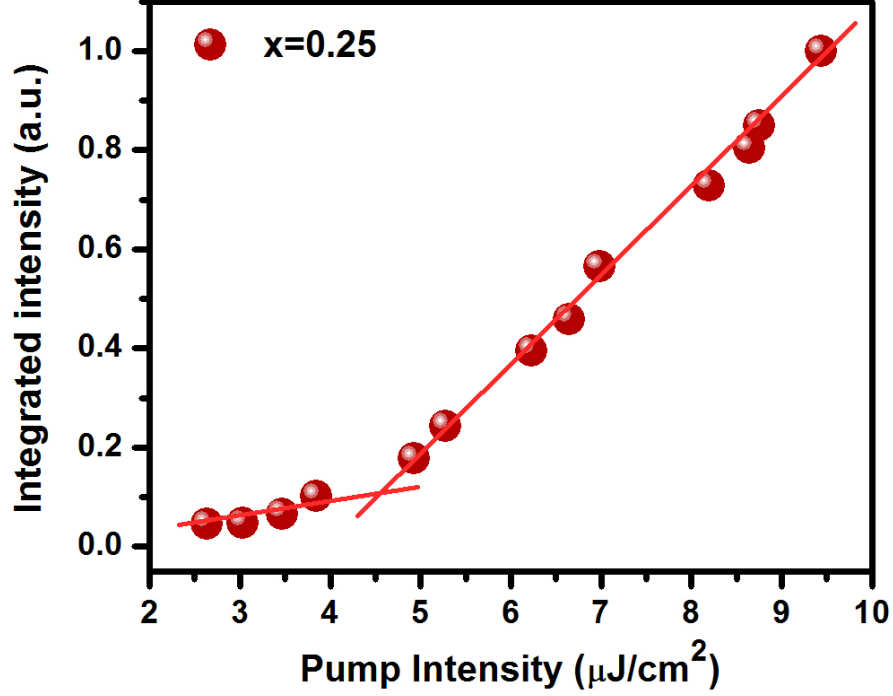
Figure 5.19: Pump intensity versus integrated intensity for our CdSe/CdSe$_{0.25}$Te$_{0.25}$/CdS core/alloyed-crown/crown NPLs.

PL integrated intensities of x=0.4 and x=0.5 are shown in Figures 5.20(a) and (b), respectively. As shown, the optical gain threshold values are 19 $\mu J/cm^2$ for x=0.4 and 13 $\mu J/cm^2$ for x=0.5.

Finally, we analyzed the optical gain loss coefficients for the CdSe/Cd$Se_{0.75}$ $Te_{0.25}$/CdS core/alloyed-crown/crown sample. To do so, we made a narrow stripe (420 μm by 130 μm) and applied a suitable optical pump intensity to observe the ASE peak. Subsequently, the sample was moved in x- and y-directions with high precision. To collect ASE intensity accurately at different distances, a fiber was closely coupled to the sample (Figure 5.21). Finally, the measured ASE intensities were numerically fitted to the relation:

$$I(\lambda) = I_0 e^{-\alpha(\lambda)l} \tag{5.5}$$

61
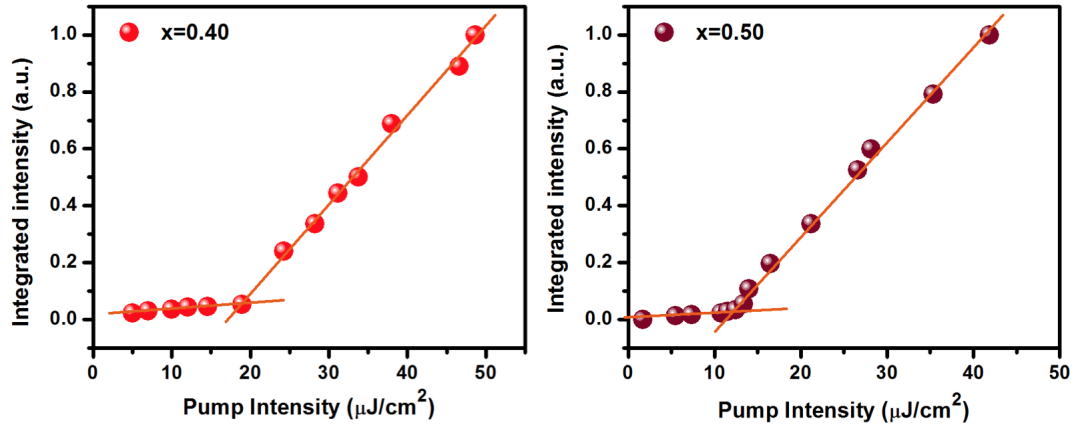
Figure 5.20: Pump intensity versus integrated intensity for our CdSe/CdSe$_{1-x}$Te$_x$/CdS NPL samples with x=0.4 and x=0.5.

In this equation, α is the optical loss coefficient, I_0 is the maximum intensity, l is the distance from the edge of the sample, and $I(\lambda)$ is the measured intensity. Here we found $\alpha = 18\ cm^{-1}$. On the other hand, in the case of bare type-II NPLs, this value was found to be $46 cm^{-1}$ [55]. This relatively low loss of the CdS coated type-II NPLs can be attributed to their nonstacking nature.
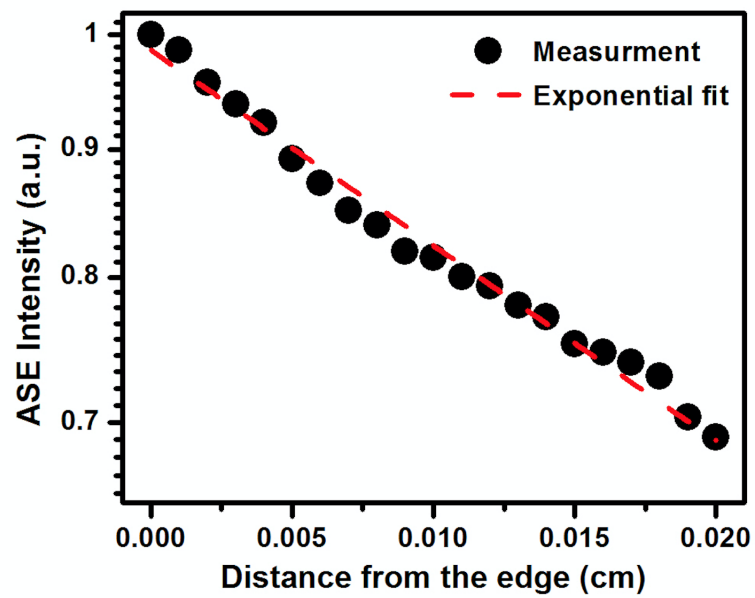
Figure 5.21: ASE intensity versus distance from the sample edge.

Chapter 6

Conclusion

Two-dimensional colloidal nanoplatelets exhibit distinguishing optical properties thanks to their atomically-flat surfaces and magic-sized vertical thicknesses. Owing to their strong quantum confinement in the vertical direction, NPLs show narrower emission linewidths compared to QDs as a result of the purely homogeneous broadening. Furthermore, since these NPLs prefer to grow only in lateral directions, they provide large linear and nonlinear absorption cross-sections. Within the scope of this thesis, two different studies on these NPLs were investigated. To understand the effect of lateral confinement, we have synthesized size-tuned NPL cores having a type-I band structure. to stabilize type-II core/alloyed-crown NPLs, we have proposed and synthesized multi-crown heterostructures.

In the size-tuned NPL study, we synthesized 4 ML thick CdSe core NPLs with different aspect ratios while keeping their lateral surface area almost constant. We performed their optical and structural characterizations to understand the effect of the lateral confinement. We hypothesized that additional confinement occurs if NPL has a width comparable to or smaller than its exciton Bohr radius. Furthermore, we measured their optical gain performances as a function of the aspect ratio for potential lasing applications.

In the multi-crown NPL heterostructures, we grew CdS around the periphery of our CdSe/CdSe$_{1-x}$Te$_x$ core/alloyed-crown NPLs to obtain highly stable type-II NPLs. We employed different material characterization methods including UV-Vis absorption, PL, and PLE spectroscopies. Also their structural properties were investigated by TEM, EDX, and XPS techniques. Our observations showed that the growth of the additional crown made of CdS around the periphery of type-II NPLs was not uniform; and instead, that CdS only grew at the edge of the CdSe/CdSe$_{1-x}$Te$_x$ core/alloyed-crown NPLs. This unsymmetrical shape of NPLs prevented the formation of stacking. In addition to these, we studied optical gain of these multi-crown heterostructures and, to the best of our knowledge, we achieved optical gain thresholds at the lowest value among all colloidal semiconductor nanocrystals.

Bibliography

[1] C. B. Murray, C. R. Kagan, and M. G. Bawendi, "Synthesis and characterization of monodisperse nanocrystals and close-packed nanocrystal assemblies," *Annual Review of Materials Science*, vol. 30, no. 1, pp. 545–610, 2000.

[2] P. van der Heide, *X-ray photoelectron spectroscopy: an introduction to principles and practices.* John & Wiley Sons, Inc, 1 ed., 2012.

[3] W. W. Brinkman, William F., Haggan, Douglas E., Troutman, "A History of the Invention of the Transistor and Where It Will Lead Us," *IEEE Journal of Solid State Circuits*, vol. 32, no. 12, pp. 1858–1865, 1997.

[4] S. Kasap and P. Capper, *Electronic and Photonic Materials.* Springer International Publishing, 2 ed., 2017.

[5] A. Ekimov, A. Efros, and A. Onushchenko, "Quantum Size Effect in Semiconductor Mircrocrystals," *Solid State Communications*, vol. 56, no. 11, pp. 921–924, 1985.

[6] A. Ekimov, A. Efros, and A. Onushchenko, "Quantum Size Effect in Semiconductor Mircrocrystals," *Solid State Communications*, vol. 56, no. 11, pp. 921–924, 1985.

[7] A. P. Alivisatos, A. L. Harris, N. J. Levinos, M. L. Steigerwald, and L. E. Brus, "Electronic states of semiconductor clusters: Homogeneous and inhomogeneous broadening of the optical spectrum," *The Journal of Chemical Physics*, vol. 89, no. 7, pp. 4001–4011, 1988.

[8] M. Bawendi, "The Quantum Mechanics Of Larger Semiconductor Clusters (," *Annual Review of Physical Chemistry*, vol. 41, no. 1, pp. 477–496, 1990.

[9] C. B. Murray, D. J. Noms, and M. G. Bawendi, "Synthesis and Characterization of Nearly Monodisperse CdE (E = S, Se, Te) Semiconductor Nanocrystallites," *Journal of American Chemical Society*, vol. 115, no. 4, pp. 8706–8715, 1993.

[10] A. P. Alivisatos, "Semiconductor Clusters, Nanocrystals and Quantum Dots," *Science*, vol. 271, pp. 933–937, 1996.

[11] X. Peng, L. Manna, W. Yang, J. Wickham, E. Scher, A. Kadavanich, and A. P. Alivisatos, "Shape control of CdSe nanocrystals," *Nature*, vol. 404, no. 6773, pp. 59–61, 2000.

[12] L. Carbone, C. Nobile, M. De Giorgi, F. Salla, A. Fiore, I. R. Franchini, M. Nadasan, A. F. Silvestre, L. Chiodo, S. Kudera, R. Cingolani, R. Krahne, and L. Manna, "Synthesis and micrometer-scale assembly of colloidal CdSe / CdS nanorods prepared by a seeded growth approach," *Nano Letters*, vol. 7, no. 10, pp. 2942–2950, 2007.

[13] S. Ithurria and B. Dubertret, "Quasi 2D Colloidal CdSe Platelets with Thicknesses Controlled at the Atomic Level," *Journal of American Chemical Society*, pp. 16504–16505, 2008.

[14] J. Ouyang, M. B. Zaman, F. J. Yan, D. Johnston, G. Li, X. Wu, D. Leek, C. I. Ratcliffe, J. A. Ripmeester, and K. Yu, "Multiple families of magic-sized CdSe nanocrystals with strong bandgap photoluminescence via noninjection one-pot syntheses," *Journal of Physical Chemistry C*, vol. 112, no. 36, pp. 13805–13811, 2008.

[15] F. Gerdes, C. Navío, B. H. Juárez, and C. Klinke, "Size, Shape, and Phase Control in Ultrathin CdSe Nanosheets," *Nano Letters*, vol. 17, no. 7, pp. 4165–4171, 2017.

[16] Y. Kelestemur, D. Dede, K. Gungor, C. F. Usanmaz, O. Erdem, and H. V. Demir, "Alloyed Heterostructures of CdSexS1-x Nanoplatelets with

Highly Tunable Optical Gain Performance," *Chemistry of Materials*, p. acs.chemmater.7b00829, 2017.

[17] M. Sharma, K. Gungor, A. Yeltik, M. Olutas, B. Guzelturk, Y. Kelestemur, T. Erdem, S. Delikanli, J. R. McBride, and H. V. Demir, "Near-Unity Emitting Copper-Doped Colloidal Semiconductor Quantum Wells for Luminescent Solar Concentrators," *Advanced Materials*, vol. 29, no. 30, pp. 1–10, 2017.

[18] Y. Altintas, M. Y. Talpur, M. Ünlü, and E. Mutlugün, "Highly Efficient Cd-Free Alloyed Core/Shell Quantum Dots with Optimized Precursor Concentrations," *Journal of Physical Chemistry C*, vol. 120, no. 14, pp. 7885–7892, 2016.

[19] D. Battaglia and X. Peng, "Formation of High Quality InP and InAs Nanocrystals in a Noncoordinating Solvent," *Nano Letters*, vol. 2, no. 9, pp. 1027–1030, 2002.

[20] M. D. Tessier, D. Dupont, K. De Nolf, J. De Roo, and Z. Hens, "Economic and Size-Tunable Synthesis of InP/ZnE (E = S, Se) Colloidal Quantum Dots," *Chemistry of Materials*, vol. 27, no. 13, pp. 4893–4898, 2015.

[21] H. V. Demir, S. Nizamoglu, T. Erdem, E. Mutlugun, N. Gaponik, and A. Eychmüller, "Quantum dot integrated LEDs using photonic and excitonic color conversion," *Nano Today*, vol. 6, no. 6, pp. 632–647, 2011.

[22] M. Achermann, M. A. Petruska, D. D. Koleske, M. H. Crawford, and V. I. Klimov, "Nanocrystal-based light-emitting diodes utilizing high-efficiency nonradiative energy transfer for color conversion," *Nano Letters*, vol. 6, no. 7, pp. 1396–1400, 2006.

[23] T. Erdem and H. V. Demir, "Semiconductor nanocrystals as rare-earth alternative," *Nature Photonics*, vol. 5, no. 3, p. 126, 2011.

[24] B. Liu, S. Delikanli, Y. Gao, D. Dede, K. Gungor, and H. V. Demir, "Nanocrystal light-emitting diodes based on type II nanoplatelets," *Nano Energy*, vol. 47, no. February, pp. 115–122, 2018.

[25] J. Lim, Y. S. Park, and V. I. Klimov, "Optical gain in colloidal quantum dots achieved with direct-current electrical pumping," *Nature Materials*, vol. 17, no. 1, pp. 42–48, 2018.

[26] B. Guzelturk, Y. Kelestemur, K. Gungor, A. Yeltik, M. Z. Akgul, Y. Wang, R. Chen, C. Dang, H. Sun, and H. V. Demir, "Stable and low-threshold optical gain in CdSe/CdS quantum dots: An all-colloidal frequency up-converted laser," *Advanced Materials*, vol. 27, no. 17, pp. 2741–2746, 2015.

[27] C.-H. M. Chuang, P. R. Brown, V. Bulović, and M. G. Bawendi, "Improved performance and stability in quantum dot solar cells through band alignment engineering," *Nature Materials*, vol. 13, no. 8, pp. 796–801, 2014.

[28] K. Wu, H. Li, and V. I. Klimov, "Tandem luminescent solar concentrators based on engineered quantum dots," *Nature Photonics*, vol. 12, no. 2, pp. 105–110, 2018.

[29] V. Klimov, *Nanocrystal Quantum Dots*. CRS Press, 1 ed., 2010.

[30] A. Ekimov, F. Hache, M. Schanne-Klein, D. Ricard, and C. Flytzannis, "Absorption and intensity-dependent photoluminescence measurements on CdSe quantum dots: assignment of the first electronic transitions," *J.Opt.Soc.Am. B*, vol. 10, no. 1, pp. 100–107, 1993.

[31] V. K. Lamer and R. H. Dinegar, "Theory, Production and Mechanism of Formation of Monodispersed Hydrosols," *Journal of the American Chemical Society*, vol. 72, no. 11, pp. 4847–4854, 1950.

[32] M. V. Kovalenko, M. Scheele, and D. V. Talapin, "Colloidal Nanocrystals with Molecular Metal Chalcogenide Surface Ligands," *Science*, no. June, pp. 1417–1420, 2009.

[33] Y. Kelestemur, B. Guzelturk, O. Erdem, M. Olutas, K. Gungor, and H. V. Demir, "Platelet-in-Box Colloidal Quantum Wells: CdSe/CdS@CdS Core/Crown@Shell Heteronanoplatelets," *Advanced Functional Materials*, vol. 26, no. 21, pp. 3570–3579, 2016.

[34] S. Ithurria, M. D. Tessier, B. Mahler, R. P. Lobo, B. Dubertret, and A. L. Efros, "Colloidal nanoplatelets with two-dimensional electronic structure," *Nature Materials*, vol. 10, no. 12, pp. 936–941, 2011.

[35] A. Polovitsyn, Z. Dang, J. L. Movilla, B. Martín-García, A. H. Khan, G. H. Bertrand, R. Brescia, and I. Moreels, "Synthesis of Air-Stable CdSe/ZnS Core-Shell Nanoplatelets with Tunable Emission Wavelength," *Chemistry of Materials*, vol. 29, no. 13, pp. 5671–5680, 2017.

[36] M. D. Tessier, P. Spinicelli, D. Dupont, G. Patriarche, S. Ithurria, and B. Dubertret, "Efficient exciton concentrators built from colloidal core/crown CdSe/CdS semiconductor nanoplatelets," *Nano Letters*, vol. 14, no. 1, pp. 207–213, 2014.

[37] S. Ithurria and D. V. Talapin, "Colloidal Atomic Layer Deposition (c-ALD) using self-limiting reactions at nanocrystal surface coupled to phase transfer between polar and nonpolar media," *Journal of the American Chemical Society*, vol. 134, no. 45, pp. 18585–18590, 2012.

[38] B. Mahler, B. Nadal, C. Bouet, G. Patriarche, and B. Dubertret, "Core/shell colloidal semiconductor nanoplatelets," *Journal of the American Chemical Society*, vol. 134, no. 45, pp. 18591–18598, 2012.

[39] C. J. de Mello, H. F. Wittmann, and R. H. Friend, "An Improved Experimental Determination of External Photoluminescence Quantum Efficiency," *Advanced Materials*, vol. 28, pp. 1741–1743, 1989.

[40] J. S. Rigden, "Macmillan encyclopedia of physics," 1996.

[41] B. Guzelturk, *Excitonics of Colloidal Nanocrystals for Next-Generation Optoelectronics.* thesis, Bilkent University, 2016.

[42] A. Yeltik, S. Delikanli, M. Olutas, Y. Kelestemur, B. Guzelturk, and H. V. Demir, "Experimental Determination of the Absorption Cross-Section and Molar Extinction Coefficient of Colloidal CdSe Nanoplatelets," *Journal of Physical Chemistry C*, vol. 119, no. 47, pp. 26768–26775, 2015.

[43] M. Li, M. Zhi, H. Zhu, W. Y. Wu, Q. H. Xu, M. H. Jhon, and Y. Chan, "Ultralow-threshold multiphoton-pumped lasing from colloidal nanoplatelets in solution," *Nature Communications*, vol. 6, pp. 1–8, 2015.

[44] E. Lhuillier, A. Robin, S. Ithurria, H. Aubin, and B. Dubertret, "Electrolyte-gated colloidal nanoplatelets-based phototransistor and its use for bicolor detection," *Nano Letters*, vol. 14, no. 5, pp. 2715–2719, 2014.

[45] Z. Chen, B. Nadal, B. Mahler, H. Aubin, and B. Dubertret, "Quasi-2D Colloidal Semiconductor Nanoplatelets for Narrow Electroluminescence," *Advanced Functional Materials*, vol. 24, pp. 295–302, 2014.

[46] A. Riedinger, F. D. Ott, A. Mule, S. Mazzotti, P. N. Knüsel, S. J. Kress, F. Prins, S. C. Erwin, and D. J. Norris, "An intrinsic growth instability in isotropic materials leads to quasi-two-dimensional nanoplatelets," *Nature Materials*, vol. 16, no. 7, pp. 743–748, 2017.

[47] Y. Chen, D. Chen, Z. Li, and X. Peng, "Symmetry-Breaking for Formation of Rectangular CdSe Two-Dimensional Nanocrystals in Zinc-Blende Structure," *Journal of the American Chemical Society*, vol. 139, no. 29, pp. 10009–10019, 2017.

[48] M. Olutas, B. Guzelturk, Y. Kelestemur, A. Yeltik, S. Delikanli, and H. V. Demir, "Lateral Size-Dependent Spontaneous and Stimulated Emission Properties in Colloidal CdSe Nanoplatelets," *ACS Nano*, vol. 9, no. 5, pp. 5041–5050, 2015.

[49] Q. Li and T. Lian, "A model for optical gain in colloidal nanoplatelets," *Chemical Science*, vol. 9, no. 3, pp. 728–734, 2018.

[50] G. H. V. Bertrand, A. Polovitsyn, S. Christodoulou, A. H. Khan, and I. Moreels, "Shape control of zincblende CdSe nanoplatelets," *Chem. Commun.*, vol. 52, pp. 11975–11978, 2016.

[51] B. Guzelturk, Y. Kelestemur, M. Olutas, S. Delikanli, and H. V. Demir, "Amplified spontaneous emission and lasing in colloidal nanoplatelets," *ACS Nano*, vol. 8, no. 7, pp. 6599–6605, 2014.

[52] Q. Li, Z. Xu, J. R. McBride, and T. Lian, "Low Threshold Multiexciton Optical Gain in Colloidal CdSe/CdTe Core/Crown Type-II Nanoplatelet Heterostructures," *ACS Nano*, vol. 11, no. 3, pp. 2545–2553, 2017.

[53] Z. Yang, M. Pelton, I. Fedin, D. V. Talapin, and E. Waks, "A room temperature continuous-wave nanolaser using colloidal quantum wells," *Nature Communications*, vol. 8, no. 1, 2017.

[54] Y. Kelestemur, M. Olutas, S. Delikanli, B. Guzelturk, M. Z. Akgul, and H. V. Demir, "Type-II colloidal quantum wells: CdSe/CdTe core/crown heteronanoplatelets," *Journal of Physical Chemistry C*, vol. 119, no. 4, pp. 2177–2185, 2015.

[55] B. Guzelturk, Y. Kelestemur, M. Olutas, Q. Li, T. Lian, and H. V. Demir, "High-Efficiency Optical Gain in Type-II Semiconductor Nanocrystals of Alloyed Colloidal Quantum Wells," *Journal of Physical Chemistry Letters*, vol. 8, no. 21, pp. 5317–5324, 2017.

[56] M. Dufour, V. Steinmetz, E. Izquierdo, T. Pons, N. Lequeux, E. Lhuillier, L. Legrand, M. Chamarro, T. Barisien, and S. Ithurria, "Engineering bicolor emission in 2D core/crown CdSe/CdSe1-xTexnanoplatelet heterostructures using band-offset tuning," *Journal of Physical Chemistry C*, vol. 121, no. 39, pp. 24816–24823, 2017.

[57] B. Abécassis, M. D. Tessier, P. Davidson, and B. Dubertret, "Self-assembly of CdSe nanoplatelets into giant micrometer-scale needles emitting polarized light," *Nano Letters*, vol. 14, no. 2, pp. 710–715, 2014.

[58] Y. Kelestemur, B. Guzelturk, O. Erdem, M. Olutas, T. Erdem, C. F. Usanmaz, K. Gungor, and H. V. Demir, "CdSe/CdSe1-xTexCore/Crown Heteronanoplatelets: Tuning the Excitonic Properties without Changing the Thickness," *Journal of Physical Chemistry C*, vol. 121, no. 8, pp. 4650–4658, 2017.